STUDIES IN NUCLEAR MAGNETIC AND NUCLEAR QUADRUPOLE RESONANCE SPECTRA

by

NORMAN GREIG CRANNA

A Thesis submitted in partial fulfilment of
the requirements for the degree of
Doctor of Philosophy
in
Physics

We accept this thesis as conforming to the standard required from candidates for the degree of Doctor of Philosophy

Members of the Department of Physics
The University of British Columbia
April 1954

ABSTRACT

Standard techniques of radio-frequency nuclear resonance spectroscopy have been applied to further studies of the interaction between atomic nuclei in crystals and the crystalline electric field gradients at the nuclear sites.

Observations have been made on the nuclear magnetic resonance spectra of Al^{27}, Li^{6}, Li^{7} and Si^{29} in single crystals of $LiAl(SiO_3)_2$ (spodumene) in strong magnetic fields. Results from the Al^{27} spectrum provided improved values of the field gradient constants of spodumene and a check on the adequacy of second and third order perturbation theory in describing the electrostatic perturbation of the magnetic energy levels; these results also provided an experimental check on a proposed new method of nuclear spin determination. The Li^{6} and Li^{7} measurements provided a more accurate value of the quadrupole moment ratio for this pair of isotopes. Observations on the Si^{29} spectrum support existing evidence that the spin of Si^{29} is 1/2.

A super-regenerative spectrometer has been built for the detection of nuclear magnetic resonances and nuclear electric quadrupole resonances. Preliminary tests indicate that it will detect resonances in solids at low frequencies

which could not be detected with the continuous-wave type of spectrometer. A pure quadrupole resonance in $Na_2B_4O_7.4H_2O$ (kernite) has been detected at 1.27 Mc./sec. using this super-regenerative spectrometer. This represents a pure quadrupole resonance of the lowest frequency reported to date.

THE UNIVERSITY OF BRITISH COLUMBIA

Faculty of Graduate Studies

PROGRAMME OF THE

FINAL ORAL EXAMINATION FOR THE DEGREE

OF DOCTOR OF PHILOSOPHY

of

NORMAN GREIG CRANNA

B. Sc. (Queen's) 1949
M. Sc. (Queen's) 1950

WEDNESDAY, MAY 5th, 1954 at 2:00 P.M.

IN ROOM 301, PHYSICS BUILDING

COMMITTEE IN CHARGE

Dean W.H. Gage - Chairman

F.A. Kaempffer	H.B. Hawthorn
J.M. Daniels	T.E. Hull
H.E.D. Scovil	V.J. Okulitch
G.M. Shrum	M.A. Ormsby

External Examiner - W.G. Proctor
University of Washington

PUBLISHED PAPERS

1. Second-Order Effects in Nuclear Electric Quadrupole Interaction of Al^{27} in Spodumene (H.E. Petch, G.M. Volkoff and N.G. Cranna), Physical Review 88, 1201, 1952.

2. Second Order Nuclear Quadrupole Effects in Single Crystals. Part II (H.E. Petch, N.G. Cranna and G.M. Volkoff) Canadian Journal of Physics, 31, 1185, 1953.

ABSTRACT

Standard techniques of radio-frequency nuclear resonance spectroscopy have been applied to further studies of the interaction between atomic nuclei in crystals and the crystalline electric field gradients at the nuclear sites.

Observations have been made on the nuclear magnetic resonance spectra of Al^{27}, Li^{6}, Li^{7} and Si^{29} in single crystals of $LiAl(SiO_3)_2$ (spodumene) in strong magnetic fields. Results from the Al^{27} spectrum provided improved values of the field gradient constants of spodumene and a check on the adequacy of second and third order perturbation theory in describing the electrostatic perturbation of the magnetic energy levels; these results also provided an experimental check on a proposed new method of nuclear spin determination. The Li^{6} and Li^{7} measurements provided a more accurate value of the quadrupole moment ratio for this pair of isotopes. Observations on the Si^{29} spectrum support existing evidence that the spin of Si^{29} is 1/2.

A super-regenerative spectrometer has been built for the detection of nuclear magnetic resonances and nuclear electric quadrupole resonances. Preliminary tests indicate that it will detect resonances in solids at low frequencies which could not be detected with the continuous-wave type of spectrometer. A pure quadrupole resonance in $Na_2B_4O_7.4H_2O$ (kernite) has been detected at 1.27 Mc./sec. using this super-regenerative spectrometer. This represents a pure quadrupole resonance of the lowest frequency reported to date.

GRADUATE STUDIES

Field of Study: Physics

Quantum Mechanics	- H.A. Elliott
Electromagnetic Theory	- W. Opechowski
Theory of Measurements	- A.M. Crooker
Nuclear Physics	- K.C. Mann
Special Relativity	- W. Opechowski
Group Theory in Quantum Mechanics	- H. Koppe

Other Studies:

Differential Geometry	- I. Halperin
Integral Equations	- T.E. Hull
Operational Methods in Engineering	- W.B. Coulthard
Physical Chemistry of High Polymers	- B.A. Dunell
Radio Chemistry	- M. Kirsch and K. Starke

THE UNIVERSITY OF BRITISH COLUMBIA

Faculty of Graduate Studies

PROGRAMME OF THE

FINAL ORAL EXAMINATION FOR THE DEGREE

OF DOCTOR OF PHILOSOPHY

of

NORMAN GREIG CRANNA

B. Sc. (Queen's) 1949
M. Sc. (Queen's) 1950

WEDNESDAY, MAY 5th, 1954 at 2:00 P.M.

IN ROOM 301, PHYSICS BUILDING

COMMITTEE IN CHARGE

Dean W.H. Gage - Chairman

F.A. Kaempffer	H.B. Hawthorn
J.M. Daniels	T.E. Hull
H.E.D. Scovil	V.J. Okulitch
G.M. Shrum	M.A. Ormsby

External Examiner - W.G. Proctor
University of Washington

PUBLISHED PAPERS

1. Second-Order Effects in Nuclear Electric Quadrupole Interaction of Al^{27} in Spodumene (H.E. Petch, G.M. Volkoff and N.G. Cranna), Physical Review 88, 1201, 1952.

2. Second Order Nuclear Quadrupole Effects in Single Crystals. Part II (H.E. Petch, N.G. Cranna and G.M. Volkoff) Canadian Journal of Physics, 31, 1185, 1953.

ABSTRACT

Standard techniques of radio-frequency nuclear resonance spectroscopy have been applied to further studies of the interaction between atomic nuclei in crystals and the crystalline electric field gradients at the nuclear sites.

Observations have been made on the nuclear magnetic resonance spectra of Al^{27}, Li^{6}, Li^{7} and Si^{29} in single crystals of $LiAl(SiO_3)_2$ (spodumene) in strong magnetic fields. Results from the Al^{27} spectrum prcvided improved values of the field gradient constants of spodumene and a check on the adequacy of second and third order perturbation theory in describing the electrostatic perturbation of the magnetic energy levels; these results also provided an experimental check on a proposed new method of nuclear spin determination. The Li^{6} and Li^{7} measurements provided a more accurate value of the quadrupole moment ratio for this pair of isotopes. Observations on the Si^{29} spectrum support existing evidence that the spin of Si^{29} is 1/2.

A super-regenerative spectrometer has been built for the detection of nuclear magnetic resonances and nuclear electric quadrupole resonances. Preliminary tests indicate that it will detect resonances in solids at low frequencies which could not be detected with the continuous-wave type of spectrometer. A pure quadrupole resonance in $Na_2B_4O_7.4H_2O$ (kernite) has been detected at 1.27 Mc./sec. using this super-regenerative spectrometer. This represents a pure quadrupole resonance of the lowest frequency reported to date.

GRADUATE STUDIES

Field of Study: Physics

Quantum Mechanics	- H.A. Elliott
Electromagnetic Theory	- W. Opechowski
Theory of Measurements	- A.M. Crooker
Nuclear Physics	- K.C. Mann
Special Relativity	- W. Opechowski
Group Theory in Quantum Mechanics	- H. Koppe

Other Studies:

Differential Geometry	- I. Halperin
Integral Equations	- T.E. Hull
Operational Methods in Engineering	- W.B. Coulthard
Physical Chemistry of High Polymers	- B.A. Dunell
Radio Chemistry	- M. Kirsch and K. Starke

ACKNOWLEDGMENTS

The research described in this thesis was supported by the National Research Council of Canada through research grants to Dr. Volkoff and through the award of Summer Scholarships (1952, 1953) and a Fellowship (1952-53) to the author. I also am grateful to the Research Council of Ontario for the award of Scholarships (1950-51, 1951-52).

To Professor Volkoff, who supervised this research, I wish to express my sincere appreciation for his active interest, for many illuminating discussions, and for his aid in numerous other ways.

I would also like to express my thanks to Mr. H. Waterman and Dr. R. Eades for helpful suggestions related to technical problems; to Mr. A.J. Fraser and Mr. W. Morrison of the Physics Department machine shop for their co-operation in constructing parts of the apparatus; to Mr. J. Sample and Mr. J. Elliott for taking the colored photograph shown in Plate I; and to Dr. R.M. Thompson of the Geology Department, Dr. B.A. Dunell of the Chemistry Department, and Dr. C.S. Samis of the Mining and Metallurgy Department, for kindly supplying crystal samples.

Finally, I wish to acknowledge the help of my wife, Maria, who has not only typed this thesis, but has contributed so much to the successful completion of this work by her constant encouragement and by shouldering so many of the parental responsibilities which should have been mine.

TABLE OF CONTENTS

LIST OF ILLUSTRATIONS

LIST OF PLATES

LIST OF TABLES

INTRODUCTION

The experimental work reported in this thesis utilizes the technique of radio-frequency nuclear resonance spectroscopy. This technique provides a method of studying the interactions between atomic nuclei and their surroundings. The work described in this thesis is confined to the case of nuclei in non-metallic crystals, subject to the following two types of interaction, one or both of which may be present:-

(a) a magnetic interaction between the nuclei and an externally applied static uniform magnetic field H_o.

(b) an electrostatic interaction between the nuclei and microscopic crystalline electric field gradients.

Part I of this thesis sets out the underlying theoretical framework. Part II reports experimental work at high magnetic fields where interactions of both types (a) and (b) are present, but (a) greatly exceeds (b). Part III reports some work at lower magnetic fields, and some at zero field where only (b) need be considered.

The experimental results so obtained yield information on both crystals and nuclei, as well as broadening the knowledge of the technique of resonance spectroscopy.

The information on crystals is related to the field gradient tensor at the sites of nuclei: the orientation

of its principal axes with respect to the crystal axes, and its degree of asymmetry, i.e. the relative magnitudes of its components along the principal axes. Such information is of particular interest to those studying the theory of bonding in solids.

The information which may be obtained about nuclei includes the determination of nuclear spins and, in the case of certain isotope pairs, the determination of quadrupole moment ratios.

The study of nuclear magnetic resonance spectroscopy is a comparatively new one, and that of nuclear quadrupole resonance spectroscopy (when $H_o = 0$) is even newer. The particular region of nuclear magnetic resonance spectroscopy where the interactions (a) and (b) are of the same order of magnitude has scarcely been touched, and any experimental results on frequencies and transition probabilities as functions of crystal orientation and magnetic field are of value in checking the existing theory, and in the planning of future experiments.

If a sample containing nuclei with spin $I \neq 0$ and magnetic moment μ is placed in a uniform magnetic field H_o, quantum mechanics predicts and experiment confirms that there will be $2I + 1$ possible orientations which the nuclei may assume with respect to H_o, and that each orientation corresponds to a definite energy level different from the

others. These are referred to as the Zeeman levels. If all other interactions between the nuclei and their surroundings are zero, or average to zero over a short time interval, the 2 I + 1 levels will be equally spaced by an amount $\mu H_o/I$. Quantum mechanics also predicts that magnetic dipole transitions due to a perturbing radio-frequency magnetic field oscillating in the plane perpendicular to H_o will only take place between adjacent levels (hence all transitions will represent the same energy difference) and therefore only provided the frequency of H_1 is equal to the classical Larmor precession frequency $\nu_o = \mu H_o / Ih$.

In the laboratory, magnetic fields as large as 10,000 gauss are comparatively easy to produce. For H_o of this order and for all nuclei of known μ, the frequencies given by the above expression fall in the range from 1 MC/sec. to 50 MC/sec. In 1946 it was shown that in a sample of protons, for example the hydrogen nuclei in water, placed in a magnetic field H_o, it was possible to induce transitions between the levels by means of a radio-frequency magnetic field H_1 perpendicular to H_o. Two independent groups, one at Stanford under Bloch (1) and one at Harvard under Purcell (2) accomplished this by different techniques and the field of nuclear radio-frequency spectroscopy was born. A great deal of information on the spin and magnetic moments of nuclei has been

compiled using these or related techniques.

This simple picture of nuclei free from interactions other than with H_o and H_1 is never strictly true, but to a good approximation it describes the situation for nuclei in solutions or liquids. Here the local magnetic field due to neighboring dipoles and any electrostatic interaction is averaged out by the thermal motion of the nuclei. Recent refined work has shown some line structure even in liquids, but we will not be concerned with this topic here.

When the samples containing nuclei are in the form of solids the picture changes somewhat. Now the nuclei, except for their vibrational energy, are in fixed positions and each nucleus experiences in addition to H_o a local magnetic field due to the neighboring dipoles. Since the dipoles are oriented in $2I + 1$ different ways the field produced at the sites of similar nuclei may vary from H_o by $\pm H_{local}$ where H_{local} can be of the order of 10 - 20 gauss or more. For example, in some crystals containing water of crystallization, two or more protons in a closely spaced group may be much nearer to each other than to other protons in similar groups. The mutual magnetic interaction of protons within a group may be strong enough to split the proton Zeeman line into components (3). However, in most cases the shift of the levels due to

variations in H_{local} is diffuse in nature and results only in a broadening of the observed Zeeman line (4).

The quadrupole moment Q of a nucleus measures the deviation from spherical symmetry of the nuclear charge distribution, being zero for the case of spherical symmetry.

If a nucleus is located in a uniform electric field $\vec{E}$, it will experience no forces or torques even when $Q \neq 0$. But if $Q \neq 0$, and at the nuclear site $\nabla \vec{E} \neq 0$, the nucleus experiences a torque and, analogous to the magnetic interaction described above, there will be a finite number of possible orientations which the nucleus may take up with respect to the gradient of the field. The inhomogeneous electric field at nuclear sites in crystals is generated by the surrounding charge distribution due to neighboring ions and the atomic electron shells and bonding electrons surrounding the nucleus itself. Quantum mechanical analysis shows the number of non-equivalent orientations, and hence the number of energy levels, to be $I + 1/2$ for the case of odd half-integral spin. The spacing of the levels involves Q, I and $\nabla \vec{E}$. The exact expression is given in the section on theory. More detailed theoretical treatment has been given by Kruger (5), Bersohn (6) and Cohen (7).

The transition frequencies between these pure quadrupole levels in the cases reported to date cover a much wider range than the Zeeman transition frequencies,

ranging from 1.5 MC/sec. to several hundred MC/sec. The pure quadrupole transition of lowest frequency up to the time of this thesis was reported by Dehmelt (8) who observed a B^{10} line in $B(CH_3)_3$ at 1.52 MC/sec. at liquid air temperature. Dehmelt has reported a great deal more work at high (9) and low frequencies (10, 11). Other results have been reported by Watkins and Pound (12), Dehmelt and Kruger (13), Dean (14), Livingstone (15) and many others. Part III of this thesis is concerned partly with reporting some new work done in this pure quadrupole field.

As can be seen from the frequency ranges of the magnetic and electric transitions mentioned above, the quadrupole interaction between a nucleus and its surroundings may be much larger than, much smaller than, or of the same order of magnitude as the magnetic interaction between the same nucleus and a H_0 of several thousand gauss. Both these interactions will be present for nuclei of spin $I \neq 0$, quadrupole moment $Q \neq 0$, contained in a crystal which has locally non-cubic symmetry, at the nuclear sites, and which is placed in a magnetic field. Since both involve the lining up of the spin axis of the nuclei they will compete with each other. At the one extreme the quadrupole interaction will be a small perturbation on the Zeeman interaction while at the other extreme the Zeeman interaction will be a small perturbation on the quadrupole interaction. Or the two interactions may be of the same order of magnitude.

A great deal of work has been reported on the quadrupole perturbation of the Zeeman levels in crystals. Carr and Kikuchi (16), Bersohn (6), Pound (17) and Volkoff et al.(18) have reported theoretical results in the field, and the latter two among others have also reported experimental results confirming the theory.

Theoretical treatments of the Zeeman perturbation of the quadrupole levels have been given to first order by Kruger (5), and Bersohn (6) calculated also the second order perturbation. Kruger and Meyer-Berkhout (19) reported observation of this effect in the quadrupole spectra of As^{75} and Dean (20) reported similar observations on Cl quadrupole spectra.

From frequency measurements on observed spectra in the above two cases, information is obtained relating to Q of the nuclei concerned and to the magnitude and orientation of $\nabla\vec{E}$ with respect to the crystal axes.

When the quadrupole and Zeeman interactions are of the same order of magnitude, perturbation theory is no longer applicable and direct but more tedious numerical calculations become necessary. Lamarche and Volkoff (21) have carried out this calculation for the particular case of Al^{27} in spodumene at one particular orientation of the crystal with respect to H_o. For this case they present complete information on the energy levels, transition

frequencies and transition probabilities for all values of H_o from zero field to high fields where the quadrupole interaction is a small perturbation on the Zeeman interaction.

Part I of this thesis outlines the theoretical framework into which the experimental work fits.

Part II describes work carried out on Al^{27}, Li^6, Li^7 and Si^{29} in spodumene in the high field region. This work was initiated with the following objects: to check the second-order and third-order perturbation theory mentioned above, to obtain higher accuracy in the values of the field gradient constants of spodumene, to check a proposed new method of spin determination which is described in the section on theory, and finally to attempt to improve the accuracy of the Q_{Li^6} / Q_{Li^7} ratio previously reported by Schuster and Pake (22). These results have already been published (23, 24).

Part III of the thesis describes work undertaken with a view to checking the above theory at zero and low magnetic fields. It was hoped to be able to present a series of observations extending from zero field to high fields so as to link the three regions described above with experimental data confirming the theory. The theoretically available signal-to-noise ratio is proportional to $H_o^{7/4}$ (25) so going to low fields presents serious difficulties. A super-regenerative spectrometer was built and with it

the Al^{27} central line in spodumene was recorded in a field of approximately 1100 gauss at a frequency of about 1.2 MC/sec. This represents an extension by a factor of 2 in frequency beyond the lower limit attained here with other types of spectrometer, and it is possible that this might be pushed another factor of 2 lower, but for a thorough study of the spectra of one type of nuclei in all 3 regions it is likely that a more suitable combination of nucleus and crystal will have to be found.

A search for the predicted pure quadrupole line of Al^{27} in spodumene has been made without success. However, a predicted pure quadrupole line of B^{11} in $Na_2B_4O_7.4H_2O$ has been recorded with this super-regenerative spectrometer at 1.27 MC/sec. This represents a pure quadrupole line of the lowest frequency reported to date. This work on B^{11} lines has not yet been submitted for publication.

PART I - THEORY

Chapter 1 - Introduction.

This part of the thesis consists of a summary of the theory of the nuclear electric quadrupole effects in nuclear resonance spectroscopy. Although none of this theory represents original work by the author of the thesis, nevertheless its inclusion is required to enable the author to interpret his experimental results presented in Parts II and III of the thesis.

We consider nuclei in single crystals and in polycrystalline solids. The magnetic resonance spectra of these nuclei will have a line width determined mainly by cell-to-cell variations of the local magnetic field due to neighboring nuclei, and perhaps by cell-to-cell variations of the electric field gradient due to crystalline imperfections and impurities. We will not consider these small perturbations further, nor will we be interested in line structure or frequency shift due to variations in local magnetic fields, diamagnetic effects, etc. We will examine the magnetic and electrostatic interactions for the cases when one or both are present and are large compared to line width.

Suppose we have a system of nuclei with spin I

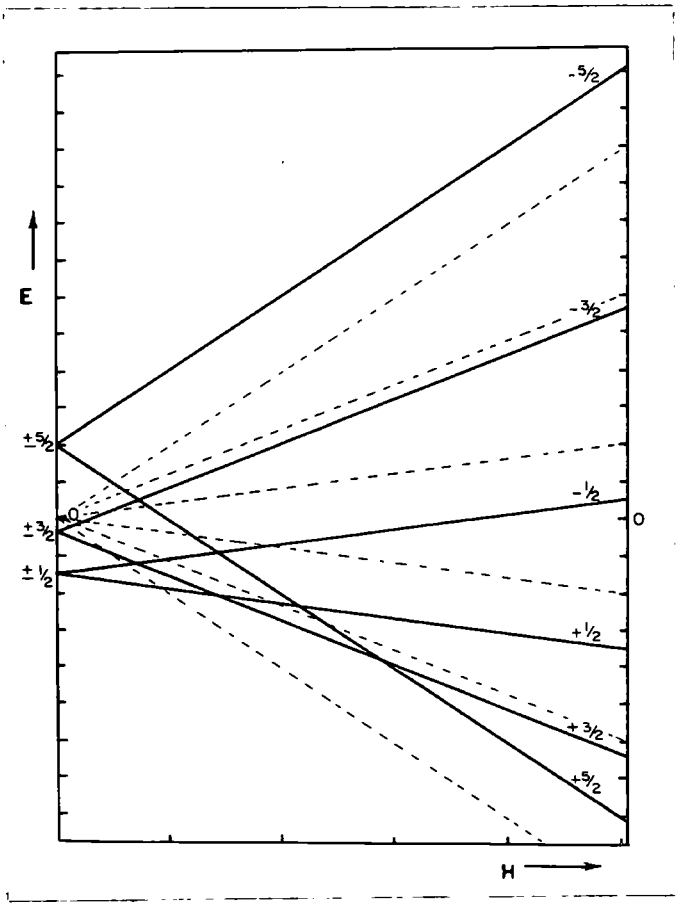

Fig. 1. Energy levels, as a function of H, for the case $I = 5/2$, $\eta = 0$ and H along the axis of symmetry of ϕ_{ij}.

to face page 11

and magnetic moment μ placed in a static magnetic field H_o. If there is no $\nabla \vec{E}$, as in sites of local cubic symmetry, then I is quantized with respect to the direction of H_o. Each eigenstate of our magnetic interaction operator $\mathcal{H} = -\vec{\mu} \cdot \vec{H}_o$ will be a pure spin-state represented by an eigenfunction, ψ_m say, where m will take the 2 I + 1 values + I, I - 1, ..., - I. The corresponding energy levels are equally spaced with spacing proportional to μH_o as shown in the dotted lines in Figure 1 for the case I = 5/2. Transitions induced by a linearly or circularly polarized r.f. magnetic field H_1 perpendicular to H_o will occur between adjacent levels only, $\Delta m = \pm 1$. Since these energy differences are the same the resonance spectrum will consist of a single line.

In the purely electrostatic case ($H_o = 0$) first consider nuclei with spin $I > 1/2$ and quadrupole moment Q, located in a crystal at sites where the field gradient has axial symmetry. This means that if we choose the axis of symmetry as the z axis, the second derivative of the electrostatic potential with respect to z, ϕ_{zz}, will be the maximum value of the field gradient; and in the plane perpendicular to the z axis, in virtue of Laplace's equation and axial symmetry, $\phi_{xx} = \phi_{yy} = -\frac{1}{2}\phi_{zz}$ regardless of the orientation chosen for the x and y axes

in this plane, The existence or non-existence of axial symmetry of $\nabla \vec{E}$ is usually described in terms of a parameter $\eta = (\phi_{xx} - \phi_{yy})/\phi_{zz}$ where these three quantities are the values of the field gradient in the direction of the three principal axes x, y, and z. The x direction is usually arbitrarily chosen to be that of the smallest value, and the z direction that of the largest value. For axial symmetry $\eta = 0$. Such conditions occur at particular sites in hexagonal and tetragonal crystals. Assume $H_0 = 0$. Then I is quantized with respect to the axis of symmetry of $\nabla \vec{E}$. Each eigenstate of our quadrupole interaction operator $\mathcal{H} = \tilde{Q} \cdot \nabla \tilde{E} = \frac{eQ\phi_{zz}}{4I(2I-1)} \left[3\vec{I}_z^2 - \vec{I}^2 \right]$ is again a pure spin-state with eigenfunction ϕ_m say, and if we restrict ourselves to the case of half-integral I, the $I + 1/2$ states will be doubly degenerate, ϕ_{+m} and ϕ_{-m} corresponding to the same energy level. This is shown in Figure I at the left where H_0 is zero. Again for a linearly or circularly polarized H_1 perpendicular to H_0, transitions occur only for $\Delta m = \pm 1$, giving a resonance spectrum of $I - 1/2$ lines. For $I = 5/2$ the frequencies of the two lines are in the ratio $2:1$. These frequencies are independent of the orientation of the crystal with respect to H_1.

Proceeding to the case where both interactions are present, the theory is simplest for the case when the axis of symmetry of $\nabla \vec{E}$ is lined up with H_0. Then the two

axes of quantization coincide and the same eigenfunctions diagonalize both $\mathcal{H}$ and $\mathcal{F}$. The total energy is simply the sum of the individual energies as shown by the solid lines in Figure I, but the differences are no longer equal. Since the eigenstates are still pure states, under the above mentioned conditions on H_1 the selection rule $\Delta m = \pm 1$ still permits transitions between adjacent levels only. But since they are of different frequencies in the general case the resonance spectrum will consist of 2 I lines.

The situation is not so straightforward if either one (or both) of the following complications is present.

(a) $\nabla \vec{E}$ is axially symmetric but this axis is not lined up with H_0.

(b) $\nabla \vec{E}$ has no axis of symmetry.

In either of these cases the eigenfunctions of the magnetic interaction $\mathcal{H}$ are not eigenfunctions of the electrostatic interaction $\mathcal{F}$ and vice versa. We must seek the eigenfunctions of the sum $\mathcal{F}+\mathcal{H}$; which will not be eigenfunctions of either $\mathcal{F}$ or $\mathcal{H}$ taken separately.

We can distinguish three cases according to the experimental situation. If $\mathcal{F} \ll \mathcal{H}$ we start with the eigenfunctions of $\mathcal{H}$ and treat the $\mathcal{F}$ operator as a perturbation. If $\mathcal{H} \ll \mathcal{F}$ we start with the eigenfunctions of $\mathcal{F}$ and treat the $\mathcal{H}$ operator as a perturbation. If $\mathcal{F}$ and

$\mathcal{H}$ are of the same order of magnitude, perturbation theory is not valid and we have to explicitly find the actual eigenfunctions of $\mathcal{F}+\mathcal{H}$. In the laboratory although we have no control over $\mathcal{F}$ once a particular crystal has been chosen we have some control over $\mathcal{H}$ since we can vary H_0, and hence in some cases we may be able to examine the spectra of a particular nuclear species in a particular crystal in all three regions.

Chapter 2 - Summary of theory as applicable to the case $\mathcal{F} \ll \mathcal{H}$.

We first introduce complication (ā) of having a $\nabla \vec{E}$ of axial symmetry with the symmetry axis not lined up along H_0. In this case, each eigenfunction perturbed by the assumed small electrostatic interaction $\mathcal{F}$, is largely the corresponding ψ_m appropriate to $\mathcal{H}$ (quantized with respect to H_0 as axis), plus a small admixture of all the other states i.e. $\chi_i = \sum_m c_m \psi_m$ where the coefficients c_m are calculable functions of the angle between the axis of symmetry of $\nabla \vec{E}$ and the quantization axis.

In the more general case of $\eta \neq 0$, the eigenfunctions are still largely the corresponding ψ_m appropriate to $\mathcal{H}$ plus a small admixture of the other states, but now the coefficients c_m are functions of η and of the angles between the principal axes and H_0. If we fix H_0 and rotate our single crystal about an axis perpendicular to H_0, we then vary these angles with resultant variations in

the c_m's and in the energy levels. It is from an analysis of this variation that we get information regarding η, the orientation of $\nabla\vec{E}$ with respect to the crystal axes and the magnitude of the quadrupole interaction energy.

A detailed theoretical treatment of this case has been given by Volkoff (26) among others. The electrostatic interaction

$$\mathcal{H} = \tilde{Q}\cdot\tilde{\nabla\vec{E}} \tag{1}$$

given by the scalar product of the nuclear electric quadrupole moment tensor with the electric field gradient tensor is regarded as a perturbation on the Zeeman energy

$$\mathcal{H} = -g\beta H_0 I_z \tag{2}$$

and in (26) the calculation is carried to the third order using standard perturbation theory. The frequency $\nu_m = |E_m - E_{m-1}|/h$ of the $m \leftrightarrow m-1$ transition is given by:

$$\frac{\nu-\nu_0}{\nu_0} = \pm\lambda(2m-1)\frac{(\nabla E)'_0}{eq} + \frac{\lambda^2}{3}P_2(m) \pm \frac{\lambda^3}{3}(2m-1)P_3(m) + 0(\lambda^4) \tag{3}$$

with

$$P_2(m) \equiv c_2(m)\left|\frac{(\nabla E)'_{\pm 2}}{eq}\right|^2 - c_1(m)\left|\frac{(\nabla E)'_{\pm 1}}{eq}\right|^2, \tag{4}$$

$$P_3(m) \equiv k_1(m)\left|\frac{(\nabla E)'_{\pm 1}}{eq}\right|^2\frac{(\nabla E)'_0}{eq} - k_2(m)\left|\frac{(\nabla E)'_{\pm 2}}{eq}\right|^2\frac{(\nabla E)'_0}{eq} - \frac{k_3(m)}{\sqrt{6}}\frac{(\nabla E)'^2_{+1}(\nabla E)'_{-2} + (\nabla E)'^2_{-1}(\nabla E)'_{+2}}{(eq)^3} \tag{5}$$

In equations (3) - (5) the primes on the components of $\nabla\vec{E}$ indicate that these are expressed in terms of the laboratory

coordinate system x', y', z' in which z' coincides with H_o. If $eq \equiv \phi_{zz}$ represents one of the eigenvalues of the tensor ϕ_{ij} then the other two eigenvalues may be written as $\phi_{xx} = -eq(1 - \eta)/2$ and $\phi_{yy} = -eq(1 + \eta)/2$. If the value of the asymmetry parameter η is restricted to the interval $0 \leq \eta \leq 1$, then $\phi_{xx}, \phi_{yy}, \phi_{zz}$ are arranged in order of increasing absolute values. However, the value of η need not be so restricted, and in that case eq is not necessarily the largest eigenvalue, but merely the eigenvalue which corresponds to that principal axis which has been arbitrarily designated as the z axis. Three quadrupole coupling constants can be defined:

$$C_z \equiv eQ\phi_{zz}/h \tag{6}$$

with corresponding expressions for C_x and C_y. The unperturbed Larmor frequency for the nucleus is given by

$$\nu_o = |\mu| H_o/hI = |\gamma| H_o/2\pi \tag{7}$$

Experimentally this frequency may be defined as the resonance frequency for the nucleus in question at a site where the time average of the electric field gradient vanishes, as is normally the case in a liquid. The dimensionless parameter λ, which is a measure of the importance of the quadrupole coupling compared to the separation of the

Zeeman levels, is defined by:

$$\lambda \equiv \frac{3C_z}{2I(2I-1)\nu_0} \tag{8}$$

The coefficients $c_i(m)$ and $k_i(m)$ in equations (4), (5) are given by:

$$\begin{aligned}
c_1(m) &= 4[(I+\tfrac{3}{2})(I-\tfrac{1}{2}) - 6(m-\tfrac{1}{2})^2], \\
c_2(m) &= 2[(I+\tfrac{3}{2})(I-\tfrac{1}{2}) - 3(m-\tfrac{1}{2})^2], \\
k_1(m) &= 12I(I+1) - 40m(m-1) - 27, \\
k_2(m) &= 2[3I(I+1) - 5m(m-1) - 6], \\
k_3(m) &= 3[8I(I+1) - 20m(m-1) - 15].
\end{aligned} \tag{9}$$

The signs of the first and third order terms of equation (3) are both to be chosen (in the case of H_0 coinciding with the + z' axis) opposite to the sign of the nuclear gyromagnetic ratio γ. As may be seen from equations (9) if m is replaced by -(m - 1), so that the -(m - 1) $\longleftrightarrow$ -m transition is considered in place of the m$\longleftrightarrow$m - 1 transition, the $c_i(m)$ and $k_i(m)$ remain unchanged. The sign of the second order term in equation (3) is therefore the same for both these transitions, while the signs of the first and the third order terms are reversed when m is replaced by -(m - 1). However, since experimentally there seems to be no way of distinguishing which one of these two transitions one is dealing with (except, in principle at least, by the use of extremely low temperatures), the sign of λ, and therefore of the quadrupole coupling constant C_z, will remain undetermined.

In the case of half integral I the resonance line

has a central component $1/2 \longleftrightarrow -1/2$, and $I - 1/2$ pairs of satellites $m \longleftrightarrow m-1$ and $-(m-1) \longleftrightarrow -m$ with $I \geqslant m > 1/2$. Such a pair shall be identified by stating the largest of the four m values involved. In the case of integral I there is no central component, but there are I pairs of satellites with $I \geqslant m > 0$. The frequency difference between the two members of each pair of satellites is given by:

$$(\nu' - \nu'')_m = 2\nu_0 \lambda (2m-1)\left[\frac{(\nabla \vec{E})'_0}{eq} + \frac{\lambda^2}{3} P_3(m) + O(\lambda^4)\right] \qquad (10)$$

The displacement with respect to the unperturbed Larmor frequency ν_0 of the center of gravity $\bar{\nu}_m \equiv (\nu' + \nu'')_m/2$ of each such pair of satellites, or of the central component, is given by:

$$\bar{\nu}_m - \nu_0 = \tfrac{1}{3}\lambda^2 \nu_0 P_2(m) + O(\lambda^4) \qquad (11)$$

As in Ref. (18) we introduce an arbitrary rectangular set of axes X, Y, Z fixed with respect to the crystal, and study the relation between the components of $\nabla \vec{E}$ in this system of axes, and in the laboratory system of axes x', y', z', as the crystal is rotated about, say, its X axis which is kept in coincidence with the y' axis perpendicular to H_0. The initial position of the crystal, in which the angle of rotation is zero, is chosen so that Y, Z coincide with z', x'. This transformation may, of

course, be obtained from the general theory of the representations of the rotation group as indicated by Bersohn (6). However, the results may also be readily obtained in an elementary way by direct substitution in terms of Cartesian coordinates following the procedure of equations (7), (8) of Ref. (18). The transformation is then given by:

$$
\begin{aligned}
(\nabla E)'_0 &= \tfrac{1}{4}(\phi_{YY} + \phi_{ZZ}) + \tfrac{1}{4}(\phi_{YY} - \phi_{ZZ})\cos 2\theta_X - \tfrac{1}{2}\phi_{YZ}\sin 2\theta_X, \\
(\nabla E)'_{\pm 1} &= \frac{1}{\sqrt{6}}[\mp\{\phi_{YZ}\cos 2\theta_X + \tfrac{1}{2}(\phi_{YY} - \phi_{ZZ})\sin 2\theta_X\} \\
&\qquad \mp i\{\phi_{XY}\cos\theta_X - \phi_{ZX}\sin\theta_X\}], \qquad (12) \\
(\nabla E)'_{\pm 2} &= \frac{1}{2\sqrt{6}}\Big[\frac{3}{2}(\phi_{YY} + \phi_{ZZ}) - \frac{1}{2}(\phi_{YY} - \phi_{ZZ})\cos 2\theta_X + \phi_{YZ}\sin 2\theta_X \\
&\qquad \pm 2i(\phi_{ZX}\cos\theta_X + \phi_{XY}\sin\theta_X)\Big].
\end{aligned}
$$

Combination of the first of equations (12) with the first order term of equation (10) leads to the following expression:

$$
\begin{aligned}
(\nu' - \nu'')_X &= \tfrac{1}{2}(2m-1)(a_X + b_X\cos 2\theta_X + c_X\sin 2\theta_X) \\
&= \tfrac{1}{2}(2m-1)[a_X + R_X\cos 2(\theta_X - \delta_X)] \qquad (13) \\
&= \tfrac{1}{2}(2m-1)[L_0 + L_1 S_X]
\end{aligned}
$$

with

$$
\begin{aligned}
a_X &\equiv L_0 + \tfrac{1}{2}L_1 = \nu_0\lambda(\phi_{YY} + \phi_{ZZ})/eq, \\
b_X &\equiv R_X\cos 2\delta_X = \nu_0\lambda(\phi_{YY} - \phi_{ZZ})/eq, \qquad (14) \\
c_X &\equiv R_X\sin 2\delta_X = -2\nu_0\lambda\phi_{YZ}/eq, \\
R_X &\equiv \tfrac{1}{2}L_1, \\
S_X &\equiv \cos^2(\theta_X - \delta_X).
\end{aligned}
$$

We may always choose δ_X in the range $-1/2\ \pi < \delta_X \leq \frac{\pi}{2}$, so as to make $R_X \geqslant 0$. A simultaneous reversal of sign of a_X, b_X, c_X and a change of δ_X by $\pi/2$ leaves $R_X \geqslant 0$. Similar expressions for the Y and Z rotations may be obtained by cyclic permutation of subscripts. The quantities

a, b, c, R, δ, L_0, L_1, are expected to be independent of m and H_0, and can be obtained from a Fourier analysis of the experimental curve of $\nu' - \nu''$ against θ .

Substitution of the last two equations (12) into equations (11) and (4) gives the extension of the above theory to the second order in λ . The second order contributes nothing new to the splitting of each pair of satellites, but gives a shift of the center of gravity $\bar{\nu}_m$ of each pair and of the central component. Thus, for the X rotation:

$$\begin{aligned}(\bar{\nu}_m - \nu_0)_X &= n_X + p_X \cos 2\theta_X + r_X \sin 2\theta_X + u_X \cos 4\theta_X + v_X \sin 4\theta_X \\ &= n_X + P_X \cos 2(\theta_X - \gamma_X) + U_X \cos 4(\theta_X - \delta_X)\end{aligned} \qquad (15)$$

Similar expressions for Y and Z rotations may be obtained by cyclic permutation of the subscripts. The coefficients n, p, r, u, v, P, U are expected to be inversely proportional to H_0, and to depend on m, and can be obtained from a Fourier analysis of the experimental curve of $\bar{\nu}_m - \nu_0$ against θ . For a rotation axis parallel to a principal axis $\gamma = \delta$ holds, and specifies the orientation of a second principal axis relative to $\theta = 0$. For a rotation axis perpendicular to a principal axis $\gamma = \delta = 0$ if θ is measured from the position in which the known principal axis is either parallel or perpendicular to H_0. In both these cases of $\gamma = \delta$ equation (15) may be rewritten in the form

$$\bar{\nu} - \nu_0 = K_0 + K_1 s + K_2 s^2 \qquad (16)$$

with $s \equiv \cos^2(\theta - \delta)$ and K_i related to n, P, U of equation (15) by:

$$\begin{aligned} n &= K_0 + \tfrac{1}{2}K_1 + \tfrac{3}{8}K_2, \\ P &= \tfrac{1}{2}(K_1 + K_2), \\ U &= \tfrac{1}{8}K_2. \end{aligned} \tag{17}$$

In a good crystal, in which all the 2I components of a resonance line are clearly visible, the nuclear spin I can be obtained simply by counting the line components. However, as will be explained in Chapter 7, crystal imperfections and impurities may so broaden and weaken the satellites that either none at all are visible, or the outer ones are so blurred and weak, that in counting the number of line components one can not be certain that none have been missed. Nevertheless, as long as the second order frequency shift of the central component and the frequency difference of only one pair of satellites (the strongest innermost pair) can be measured, the nuclear spin can be determined from a rotation about any arbitrary axis by combining the experimental values of U from equation (15) for the central component (m = 1/2), and of R from equation (13) for the innermost pair of satellites (m = 3/2) in the expression

$$(I + \tfrac{3}{2})(I - \tfrac{1}{2}) = 32\nu_0 U/R^2. \tag{18}$$

Here ν_0 is the unperturbed Larmor frequency corresponding

to the value of H_o at which U has been measured. The product $\nu_o U$ should be independent of H_o.

If the orientation of some one of the principal axes of ϕ_{ij} is known from crystal symmetry we can use it as the X rotation axis, and choose Y and Z rotation axes in the plane perpendicular to it. We choose the X and Y axes to coincide respectively with the b and c axes of spodumene. If we do not restrict the value of the asymmetry parameter $\eta = (\phi_{xx} - \phi_{yy})/\phi_{zz}$ to the range $0 \leqslant \eta \leqslant 1$ we may name the principal axes at will. We shall choose the principal axis coincident with the X rotation axis as the x principal axis corresponding to the eigenvalue $\phi_{xx} = -1/2(1 - \eta)\phi_{zz}$. The y and z principal axes must then lie in the YZ plane. Let δ denote the angle between the Y rotation axis and the y principal axis corresponding to the eigenvalue $\phi_{yy} = -1/2(1 + \eta)\phi_{zz}$. A positive δ will mean that a positive rotation of the crystal about the X axis will bring the yz axes into the position originally occupied by the YZ axes. To analyze the experimental data completely we must determine δ, η, and the absolute value of the Quadrupole coupling constant referred to the z axis $|C_z| \equiv |eQ\phi_{zz}/h|$. For I = 5/2 the latter two quantities are related to a_x and R_x of equation (13) by:

$$\eta = 1 + \frac{4a_x}{R_x - a_x}, \quad |C_z| = \tfrac{10}{3}|R_x - a_x|. \tag{19}$$

Since the Y and Z axes are known to be perpendicular to a principal axis, $c_Y = c_Z = 0$ and $\delta_Y = \delta_Z = 0$. If satellites are visible, then a_Y, $b_Y = R_Y$, a_Z, $b_Z = R_Z$ are obtainable directly from an analysis of the experimental curves of the form of equation (13), and a check on a_X and $b_X = R_X \cos 2\delta$ may be obtained with the aid of the identities:

$$a_X = \tfrac{1}{2}(b_Y - a_Y) = -\tfrac{1}{2}(b_Z + a_Z)$$
$$b_X = -\tfrac{1}{2}(3a_Y + b_Y) = \tfrac{1}{2}(3a_Z - b_Z) \qquad (20)$$

If $|C_Z|$, η, and δ are known from one rotation, the values of $\nu' - \nu''$ and $\bar{\nu} - \nu_o$ for other rotations are easily computed. The following formulae for the case of $I = 5/2$. are quoted since they will be required in Chapter 6.

The first order frequency splitting for the X, Y rotations are given by the last of equations (13) with the coefficients L_o, L_1 determined by:

$$\text{X:}\quad L_o = \tfrac{3}{10}C_Z \quad , \; L_1 = -\tfrac{3}{20}C_Z(3 + \eta)$$
$$\text{Y:}\quad L_o = -\tfrac{3}{20}(1 - \eta)C_Z, \; L_1 = \tfrac{3}{20}\left[(3 + \eta)\cos^2\delta - 2\eta\right]C_Z \qquad (21)$$

The second order frequency shifts of the inner satellites for the Y rotation is given by equation (16) with the

coefficients K_i as follows:

$$K_0 = \frac{5}{8}(3+\eta)^2 C_z^2/800\nu_0$$
$$K_1 = -\frac{3}{4}\left[2\eta(5+7\eta)+13(3+\eta)(1-\eta)\cos^2\delta\right] C_z^2/800\nu_0 \qquad (22)$$
$$K_2 = \frac{21}{8}\left[2\eta-(3+\eta)\cos^2\delta\right]^2 C_z^2/800\nu_0$$

The third order contribution to the frequency splitting for the rotation is given for the "inner" satellites (m = 3/2) by:

$$\frac{9}{2000}\frac{C_z^3}{\nu_0^2}\Big[-\frac{11}{16}\eta^2 + s_X(3+\eta)\frac{288+402\eta+113\eta^2}{96} - s_X^2(3+\eta)^2\frac{251+44\eta}{64} + s_X^3(3+\eta)^3\frac{385}{384}\Big] \qquad (23)$$

and for the "outer" satellites (m = 5/2) by:

$$\frac{9}{1000}\frac{C_z^3}{\nu_0^2}\Big[-\frac{1}{16}\eta^2 - s_X(3+\eta)\frac{432+258\eta+37\eta^2}{96} + s_X^2(3+\eta)^2\frac{279+86\eta}{64} - s_X^3(3+\eta)^3\frac{365}{384}\Big]. \qquad (24)$$

Equations (21), (23), (24) give the correct relative sign of the first and third order contributions to $\nu' - \nu''$, but the absolute sign will remain undetermined.

Chapter 3 - Theory for the pure quadrupole case ($H_0 = 0$).

The quadrupole interaction operator given in equation (1) can be reduced to the following Hamiltonian(13)

$$\mathcal{H} = \frac{eQ\phi_{zz}}{4I(2I-1)}\left[(3\vec{I}_z^2 - \vec{I}^2) + (\vec{I}_x^2 - \vec{I}_y^2)\eta\right] \qquad (25)$$

where x, y, and z are the principal axes of ϕ_{ij} , $\vec{I}$ is the angular momentum operator and Q is the scalar nuclear quadrupole moment defined in the conventional manner (27)

$$eQ = \left(II\left|\sum_i e r_i^2 (3\cos^2\theta_{iz} - 1)\right|II\right) \qquad (26)$$

In the case of half-integral I the secular determinant

$$\left|\mathcal{H}_{mm'} - E\,\delta_{mm'}\right| = 0 \qquad (27)$$

can be factored into two determinants each of which leads to a characteristic equation of degree I + 1/2 (21). The eigenstates defined by each of these sub-determinants are linear combinations of one of two subsets into which the functions ψ_m which diagonalize I_z may be subdivided. One set, L say, includes ψ_m with m = 1/2 + 2n and the other, M say, includes ψ_m with m = -1/2 + 2n, where n is an integer.

The eigenvalues are still doubly-degenerate as

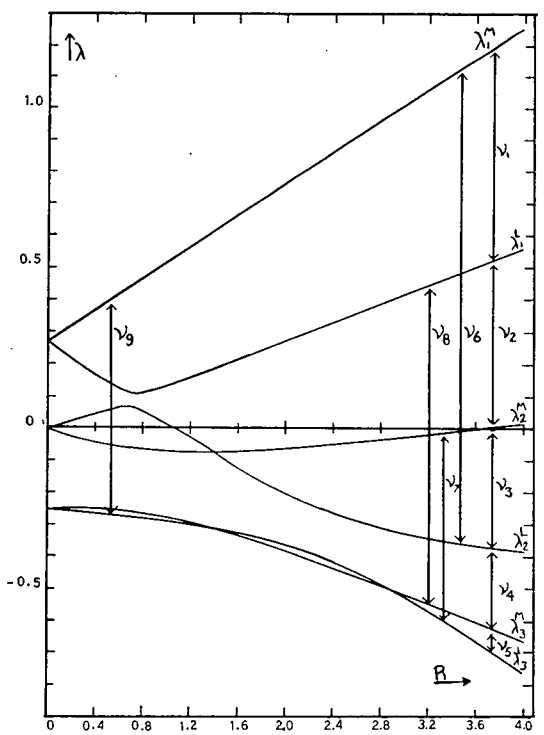

FIG. 2. Energy values for $I = 5/2$, $\eta = 0.95$ in terms of $\lambda \equiv E/eQ\phi_{zz}$ as a function of $R \equiv 4\mu H_0/eQ\phi_{zz}$, for $0 \leqslant R \leqslant 4$. H_0 is along the z principal axis of ϕ_{ij}. The arrows represent the possible absorption lines, and are numbered from 1 to 9, the first five being the Zeeman transitions for $R \gg 1$.

to face page 26

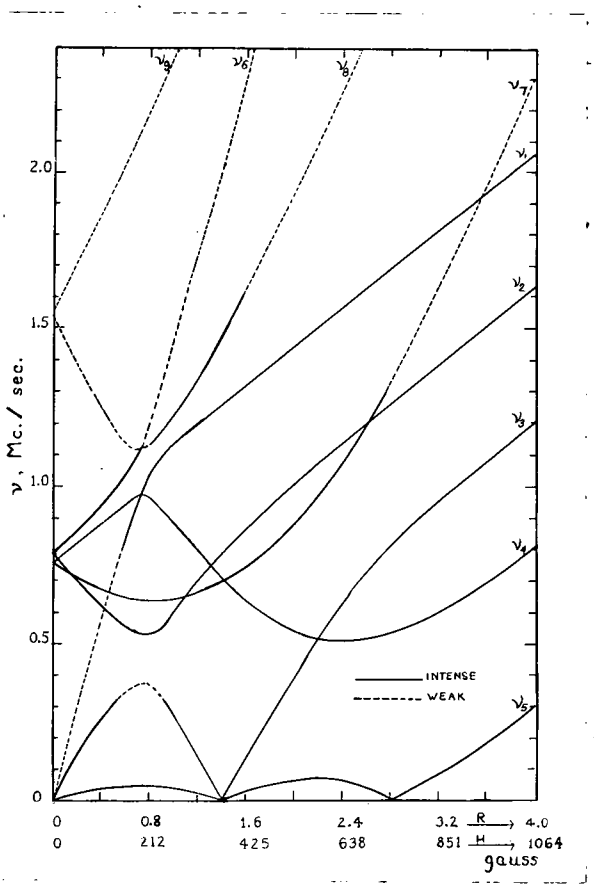

Fig. 3. Transition frequencies ν (in Mc./sec.) as a function of R (or of $H_0 = ReQ\phi_{zz}/4\mu$). Lines have been labelled intense or weak in accordance with relative values of the squares of matrix elements being greater or smaller than unity on the arbitrary scale used in Fig. 4.

to face page 26

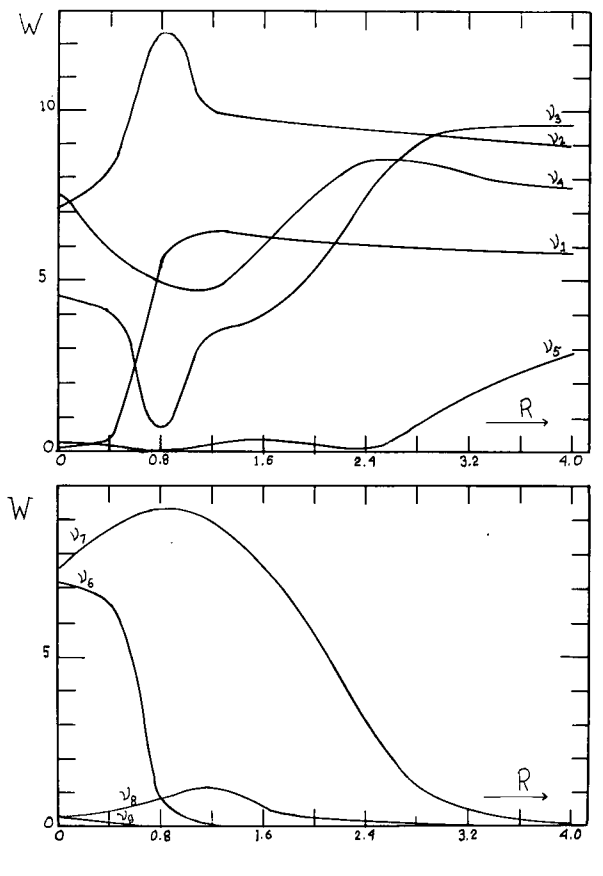

Fig. 4. Squares of the matrix elements of the perturbing operator (in arbitrary units) as a function of $R = 4\mu H_0/eQ\phi_{zz}$.

to face page 26

for $\eta = 0$. For I = 5/2 the secular equation resulting from (27) is

$$\lambda^3 - \frac{1}{400}(7\eta^2+21)\lambda - \frac{1}{400}(1-\eta^2) = 0 \qquad (28)$$

where $\lambda \equiv E/eQ\phi_{zz}$. When η and the quadrupole coupling constant are known from magnetic resonance spectra, the roots of this equation will give the pure quadrupole energy levels. Lamarche (28) gives approximate expressions for the roots of equation (28) for small η. For $\eta = 0.94$ as at the Al^{27} sites in spodumene, one root is negative and very nearly zero and the other two, one positive and one negative, are nearly equal in absolute value giving transition frequencies of .758 MC/sec. and .789 MC/sec. For small η Townes and Dailey (29) give $2(1 - 1.30\,\eta^2)$ as the approximate expression for the ratio of the two frequencies. Another feature differing from the $\eta = 0$ case is that due to the eigenstates being admixtures of states there is a finite probability of a transition occurring at the sum of these frequencies. Figures 2 and 3 taken from Ref. (21) represent the dependence of the energy levels and the transition frequencies on the magnetic field H_o. Figure 4 is a revised version of the corresponding figure of Ref. (21). The situation described above for the zero field case corresponds to the

left hand side of each of these Figures. In Figure 2, note that the vertical scale represents energy in units of the quadrupole coupling constant times h, while the horizontal scale is the ratio of the magnetic interaction energy μH_0 to the quadrupole interaction energy $eQ\phi_{zz}/4$. Recent unpublished calculations by Lamarche & Volkoff have shown that, while the transition frequencies are independent of the orientation of the r.f. field H_1 with respect to the crystal, the transition probabilities are strongly dependent on this orientation. In the case of Al^{27} in spodumene the relative transition probabilities for the .758 MC/sec. line for H_1 along the x, y and z principal axes of the ϕ_{ij} tensor at the Al sites are in the ratio of 70 : 25 : 5.

Chapter 4 - Theory applicable to the region where $\mathcal{F} \simeq \mathcal{H}$.

In Ref. (21) Lamarche & Volkoff report the result of some calculations for the case of Al^{27} in spodumene. These calculations include the case $H_0 = 0$ and the particular case of H_0 coinciding with the z principal axis of the ϕ_{ij} tensor for all values of H_0 from zero up to the region where perturbation theory based on $\mathcal{F} \ll \mathcal{H}$ becomes

accurate. This calculation involved the solving of the secular determinant

$$\left|(\mathcal{F}+\mathcal{H})_{mm'}-E\,\delta_{mm'}\right|=0 \qquad (29)$$

for the energy levels and the computing of the frequencies and the relative transition probabilities between them. The results are shown in Figures 2, 3 and 4. The classification of eigenfunctions described in Chapter 3 persists when H_o is applied along the z principal axis of $\nabla\vec{E}$, each L class eigenfunction now becoming a linear combination of $\psi_{-3/2}$, $\psi_{1/2}$ and $\psi_{5/2}$, and each M class eigenfunction a linear combination of $\psi_{-5/2}$, $\psi_{1/2}$ and $\psi_{3/2}$. The coefficients in each case are functions of H_o, and the character of some of the eigenstates changes markedly as the field is varied. For example in Figure 2, while λ_1^M maintains mostly the character of $\psi_{-5/2}$ throughout, λ_2^L which has mainly the character of $\psi_{-1/2}$ at high fields, changes to mainly $\psi_{-5/2}$ in the region of R = 0.8 to 1.8 and then becomes chiefly $\psi_{+3/2}$ as zero field is approached. Note that the energy levels corresponding to eigenstates of different classes do cross but those corresponding to eigenstates of the same class do not cross. The $\Delta m=\pm 1$ rule now indicates that transitions can occur between any pair of levels belonging to different classes. The resultant transition frequencies

are plotted vs. R in Figure 3.

At high fields the eigenstates are chiefly those appropriate to $\mathcal{H}'$ (quantized with respect to H_0 as axis) and only the five transitions designated ν_1 to ν_5 have sufficient probability to make the resultant spectral lines observable. But as the ratio R gets below 3 the percentage of the other spin functions in the linear combination characterizing the states becomes appreciable. The relative transition probabilities for the other four possible transitions, labelled ν_6 to ν_9 , shown in Figure 4 indicate that they should be observable in certain regions.

The effect, on the observed nuclear resonance spectrum, of rotating the crystal at zero magnetic field and at high magnetic fields has been described. In the region where $\mathcal{F} \approx \mathcal{H}'$, rotation of the crystal so that H_0 is not along a principal axis of $\nabla \vec{E}$ will in general result in the eigenfunctions belonging to the various levels becoming linear combinations of all the spin functions. Then in principle transitions can occur between any pair of levels and a total of 15 combinations are possible for the I = 5/2 case. Many of these will not be observable because of low frequencies or low transition probabilities.

PART II - EXPERIMENTAL

Extension of Results in Spodumene at high Magnetic Fields.

Chapter 5 - Apparatus and Experimental Procedure.

The recording nuclear magnetic resonance spectrometer, the electromagnet, and the crystal mount used in the work described in this part of the thesis have been described fully in Refs. (18, 30). The two crystal samples of $LiAl(SiO_3)_2$ (spodumene) used have also been described elsewhere (23). One, designated 2Y, has a volume of about 1.3 c.c. and was rotated about the crystal "c" axis which coincides with the arbitrarily chosen Y axis mentioned in Chapter 2. This crystal was oriented with respect to the holder by means of the experimental curve obtained for the splitting of the inner satellites. This was adjusted to make $\theta_Y = 0$ correspond to the position of maximum splitting. The other, designated 3X, has a volume of about 1.5 c.c. and was rotated about the crystal b axis which coincided with the arbitrarily chosen X axis mentioned in Chapter 2. This crystal was oriented with respect to the holder using two well-defined cleavage planes. Their intersection defined the c axis and the bisector of the angle between these planes, lying perpendicular to the c axis, defined the b axis.

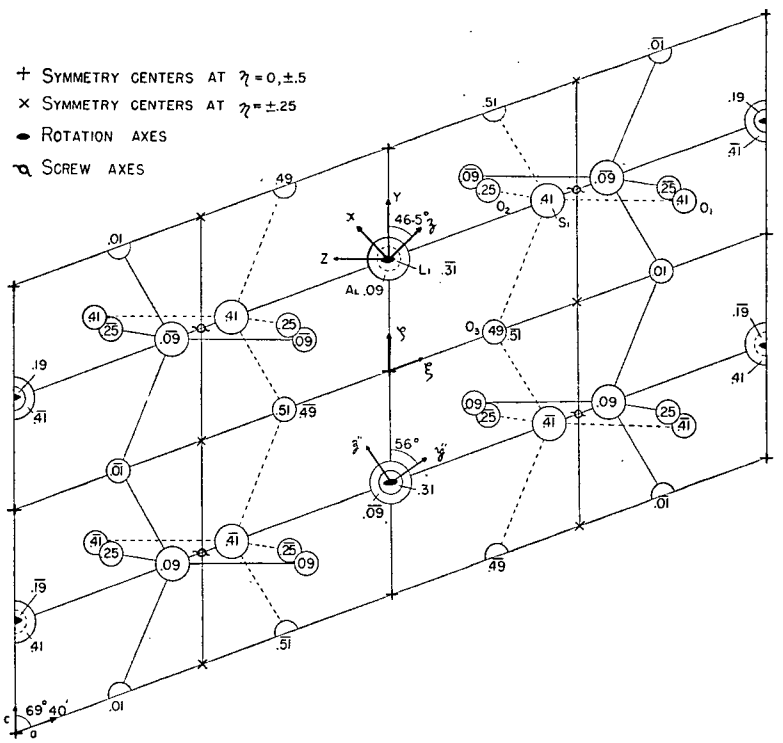

FIG. 5. Projection of a unit cell of monoclinic spodumene on the (010) plane. The b axis, which is perpendicular to the page, was used as the X rotation axis, and coincides with the y and x'' principal axes of the field gradient tensors ϕ_{ij} at the Li and Al sites respectively. The Y and Z rotation axes, and the x, z and y', z'' principal axes of ϕ_{ij} at the Li and Al sites respectively are shown in the diagram.

to face page 31

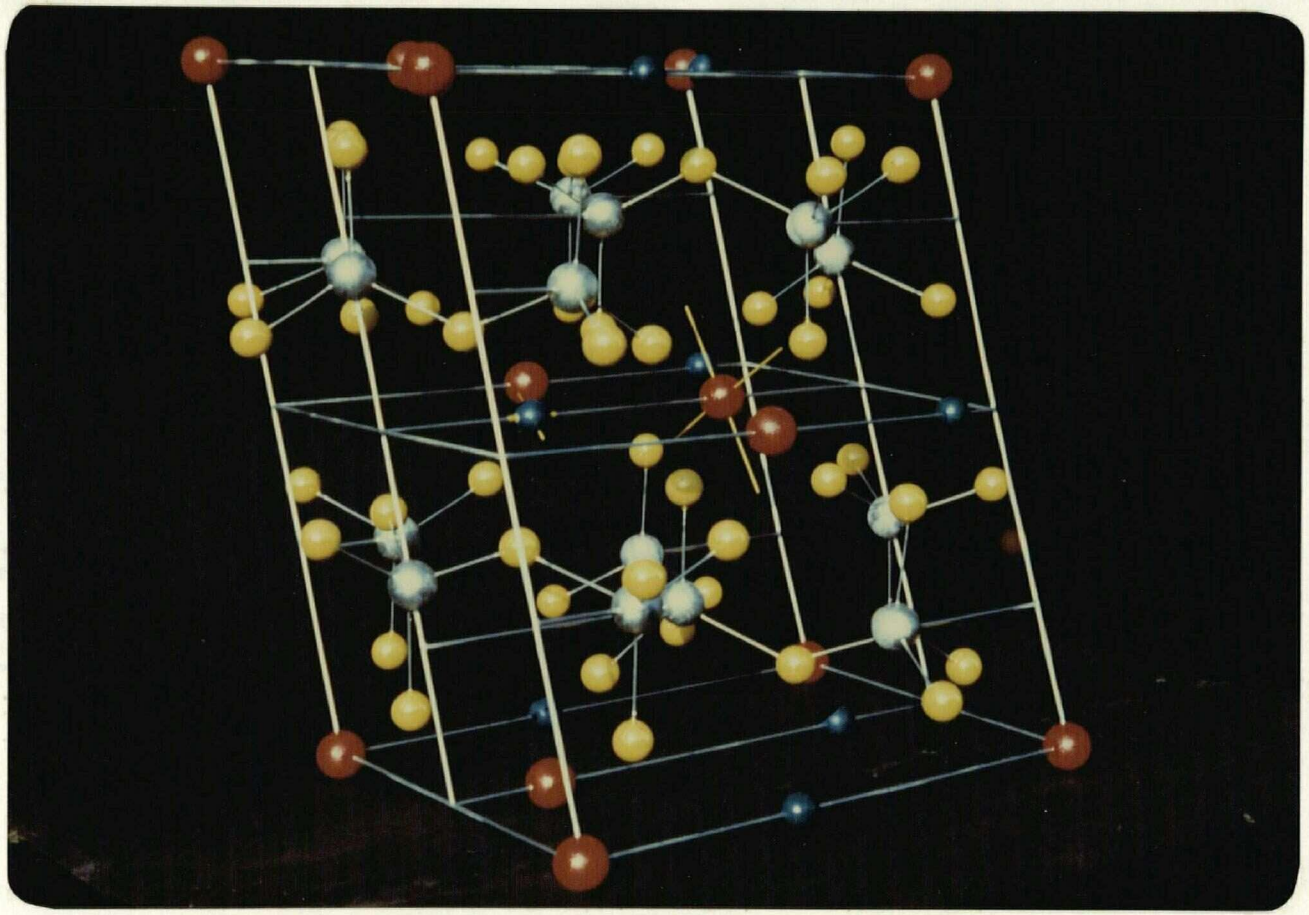

PLATE I. Color photograph of a 3 - dimensional model of the $LiAl(SiO_3)_2$ (spodumene) unit cell. Al, Li, Si and O nuclei are represented respectively by the red, blue, silver and yellow balls. On the central Al and Li nuclei the yellow lines indicate the directions of the y and z principal axes of the field gradient tensor at each of these sites as determined experimentally in this laboratory.

to face page 31

A projection of the structure of spodumene on the (010) plane is given in Fig. 5. A detailed description of the structure is given in Ref. (18). A color photograph of a 3-dimensional model of the unit cell is shown in Plate I. The Li, Al, Si and O nuclei are represented respectively by the blue, red, silver and yellow balls.

Frequency measurements were made using either a General Radio 620A Frequency Meter or a BC-221 A Frequency Meter, and a communications receiver. Regular frequency markers were made on the chart by zero beating the spectrometer oscillator with the frequency meter. Frequencies corresponding to zero derivative were then measured directly from the charts using linear interpolation between these markers. Where a knowledge of ν_o was essential as in the $\bar{\nu}_m - \nu_o$ curves, ν_o was checked periodically by removing the crystal and inserting a test tube of aluminum chloride solution. In the experimental results in section A and B below it is estimated that the individual frequencies could be measured to $\pm$ 1 KC/sec. and the angular positions of the crystal sample to $\pm$ 1/2° relative to an arbitrary zero on the crystal mount scale whose position with respect to the magnetic field could in turn be determined to $\pm$ 1°.

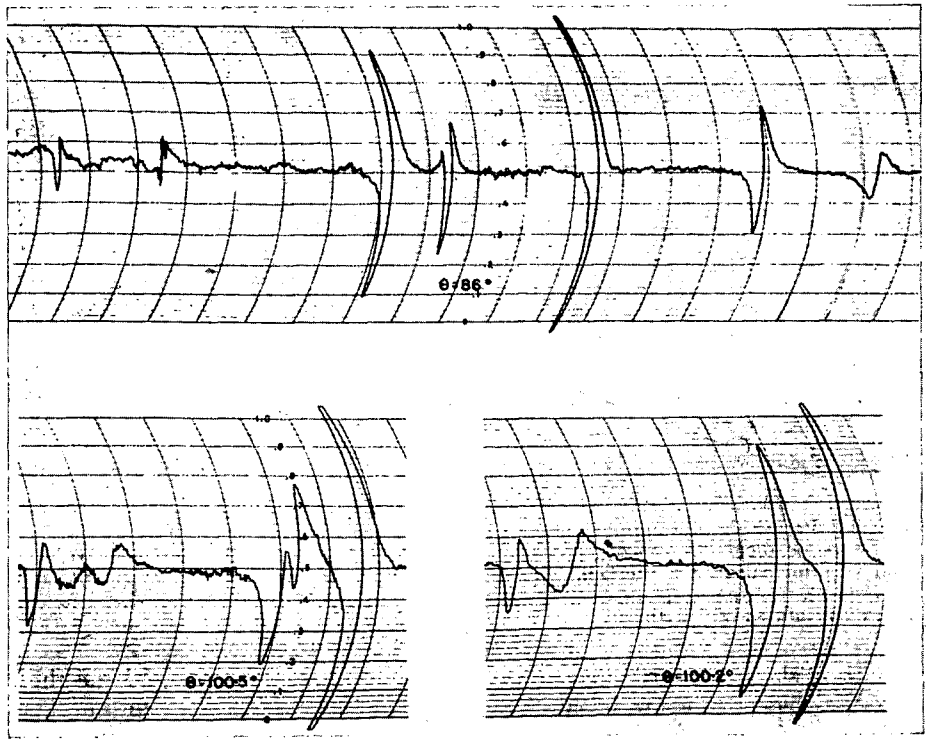

FIG. 6. Selected traces of the recorded derivative of the Al^{27} absorption line in spodumene sample No. 3X at $H_0 = 6130$ gauss corresponding to $\nu_0 = 6.806$ Mc./sec. (*a*) $\theta_X = 86°$. Sweep rate is approximately 54 kc./sec. per division. The lines and their approximate frequencies in Mc./sec. are from right to left: "outer" satellite of Al^{27} line 6.458, "inner" satellite 6.585, central component 6.769, Cu^{63} line 6.930, second "inner" satellite 7.009, second "outer" satellite 7.307, Cu^{65} line 7.420. The Cu lines are not symmetric because some dispersion mode is mixed in with the absorption mode owing to the phase shift of the H_1 r-f. field penetrating the metal of the oscillator coil. The more abundant Cu^{63} isotope gives the stronger line. (*b*) $\theta_X = 100.2°$. Sweep rate is approximately 27 kc./sec. per division. The lines and their approximate frequencies in Mc./sec. are from right to left: central component of Al^{27} line 6.756, the two coalesced "inner" satellites 6.794, the two coalesced "outer" satellites 6.903, Cu^{63} line 6.930. (*c*) $\theta_X = 100.5°$. Same as *b*, except that both pairs of coalesced satellites have begun to split up.

to face page 32

Chapter 6 - Experimental Results and Calculations.

A. Inner satellites of Al^{27} in spodumene.

The results on the inner satellites in conjunction with Petch's (31) results on the Al^{27} central line were recently published (23). They are presented below much as they appeared in Ref. (23). In making the final calculations for the constants of spodumene the best experimental values were chosen from both sets of results. In reproducing this material those parts of Petch's results incorporated in the calculations are necessarily included.

The following theoretical conclusions were verified. (a) If, and only if, second and higher order effects are negligible a crystal position can be found for which all the line components simultaneously coalesce at the unperturbed Larmor frequency ν_0 . In the Al^{27} line in spodumene the components do not all coalesce for any crystal position, indicating an appreciable second order effect. (b) In the absence of measurable third order effects, but irrespectively of the presence or absence of second order effects, the first order splitting $\nu' - \nu''$ between two members of a pair of satellites should vanish in a crystal position which is the same for all satellite pairs for a given line, and which is independent of H_0. Fig. 6 shows representative traces obtained with sample No. 3X, described in Chapter 5, in three positions in a magnetic field of

H_0 = 6130 gauss, calculated from the known gyromagnetic ratio for Al^{27} and the measured value of ν_0 = 6.806 MC/sec. for Al^{27} in aluminum chloride in solution. At $\theta_X = 86°$ the five components of the Al^{27} line are widely separated and are clearly visible in addition to the two lines due to Cu^{63} and Cu^{65} in the oscillator coil winding. As the crystal is rotated about its b axis (chosen as the X rotation axis) the copper lines remain at their fixed frequencies, while the components of the Al^{27} line gradually change their position. By the time $\theta_X = 100.2°$ has been reached the lower frequency member of each pair or satellites has crossed over to the high frequency side of the central component, and has coalesced with the other member of the same pair as shown in Fig. 6b. The coalesced pairs lie at frequencies recorded in Table 1.

TABLE I

DEPENDENCE ON THE MAGNETIC FIELD H_0 OF THE FREQUENCY SHIFT $\bar{\nu} - \nu_0$ OF THE CENTRAL COMPONENT AND OF THE CENTERS OF GRAVITY $\bar{\nu} - \nu_0 = \frac{1}{2}(\nu' + \nu'') - \nu_0$ OF THE "INNER" AND "OUTER" SATELLITES OF THE Al^{27} LINE IN SAMPLE No. 3X IN THE POSITION $\theta_X = 100°$ IN WHICH THE SPLITTING $\nu' - \nu''$ OF THE SATELLITE PAIRS VANISHES

ν_0, Mc./sec.	H_0, gauss	$1/\nu_0$, relative	Central component ($m = \frac{1}{2}$)			"Inner" satellites ($m = 3/2$)			"Outer" satellites ($m = 5/2$)		
			$\bar{\nu}$, Mc./sec.	$\bar{\nu} - \nu_0$, Mc./sec.	$\bar{\nu} - \nu_0$, relative	$\nu' = \nu'' = \bar{\nu}$, Mc./sec.	$\bar{\nu} - \nu_0$, Mc./sec.	$\bar{\nu} - \nu_0$, relative	$\nu' = \nu'' = \bar{\nu}$, Mc./sec.	$\bar{\nu} - \nu_0$, Mc./sec.	$\bar{\nu} - \nu_0$, relative
3.662	3300	1.000	3.570	−.092 ±.001	1.000	3.643	−.019 ±.001	1.000	3.843	.181 ±.001	1.000
6.806	6130	0.539	6.756	−.050 ±.001	0.54 ±.01	6.794	−.012 ±.001	0.63 ±.06	6.903	.097 ±.001	0.535 ±.005
9.884	8903	0.371	9.849	−.035 ±.001	0.38 ±.01	9.876	−.008 ±.001	0.42 ±.05	9.952	.068 ±.001	0.376 ±.005

A further small rotation of the crystal to $\theta_X = 100.5°$ already produces a noticeable tendency of both coalesced

satellite pairs to split as shown in Fig 6c. Thus the position of zero splitting can be found with considerable accuracy, and as expected turns out to be the same for both the "inner" (m = 3/2) and the "outer" (m = 5/2) satellite pairs. The magnetic field was then changed to H_o = 3300 gauss and H_o = 8903 gauss, corresponding to ν_o = 3.662 Mc./sec. and ν_o = 9.884 Mc./sec. respectively. The position of zero splitting was determined for each of the three values of H_o used, and was found to differ by not more than 1/2° between the two extreme values of H_o used. This indicates that third order effects must be quite small at this crystal position.

(c) In the absence of measurable fourth order effects the magnitude of the second order frequency shift $\bar{\nu} - \nu_o$ of the central component, or of the center of gravity of a pair of satellites, should be inversely proportional to H_o for a given crystal position, and for a given line component should have the same form of dependence on the angular position of the crystal independently of H_o. Sample No. 3X was used to obtain the data recorded in Table I corresponding to the one position in which the first order splitting vanished for both satellite pairs, so that $\nu' = \nu'' = \bar{\nu}_m$ in both cases. In all cases $\bar{\nu} - \nu_o$ is inversely proportional to ν_o within experimental error.

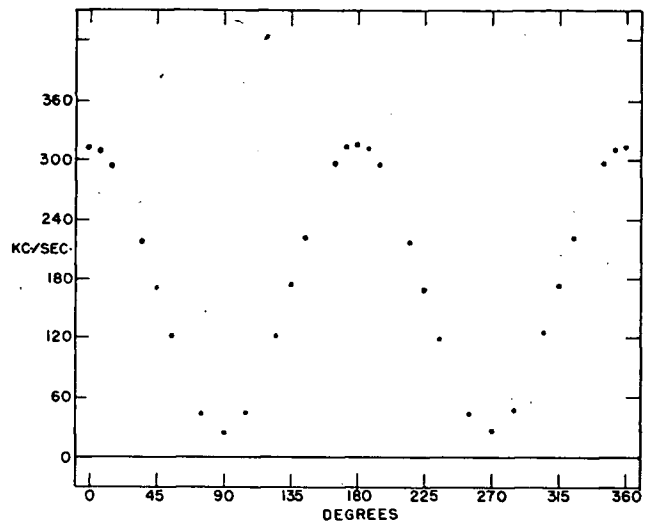

FIG. 7. Dependence on the angular position of spodumene sample 2Y of the frequency difference $\nu' - \nu''$ of the "inner" satellites of the Al^{27} line for the Y rotation about the crystal c axis. $\theta_Y = 0$ corresponds to the position of the crystal in which the b axis is at 90° to the magnetic field H_0. $H_0 = 5862$ gauss, corresponding to $\nu_0 = 6.508$ Mc./sec.

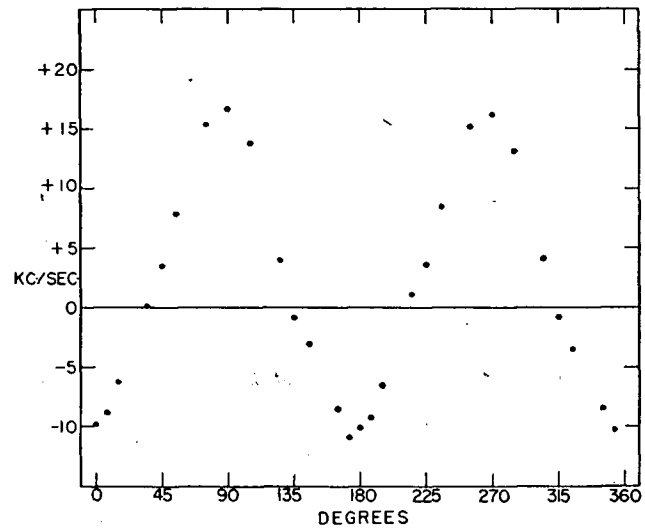

FIG. 8. Dependence on the angular position of spodumene sample 2Y of the frequency shift $\bar{\nu} - \nu_0 = \frac{1}{2}(\nu' + \nu'') - \nu_0$ of the center of gravity of the "inner" satellites of the Al^{27} line for the Y rotation about the crystal c axis. $\theta_Y = 0$ corresponds to the position of the crystal in which the b axis is at 90° to the magnetic field H_0. $H_0 = 5862$ gauss, corresponding to $\nu_0 = 6.508$ Mc./sec.

to face page 35

Figs. 7 and 8 represent respectively the experimental values of $\nu' - \nu''$ and $\bar{\nu} - \nu_o = 1/2(\nu' + \nu'') - \nu_o$ for the "inner" ($m = 3/2$) satellites of the Al^{27} line as a function of θ_Y for the Y rotation of sample No. 2Y. The magnetic field H_o was held constant at approximately 5862 gauss corresponding to the observed Larmor frequency for Al^{27} in aluminum chloride of $\nu_o = 6.508$ MC/sec. The zero of the θ_Y scale should be chosen at that position of the crystal in which the X(or b) axis is perpendicular to H_o. This position was accurately located by making the observed $\nu' - \nu''$ curve of Fig. 7 symmetrical about this point. This same crystal position was also chosen for $\theta_Y = 0$ for the $\bar{\nu} - \nu_o$ curve of Fig. 8. Since the accuracy of each experimental point is $\pm$ 1 kc./sec., and the total variation of the curve is less than 30 kc./sec., any seeming lack of symmetry of this curve about $\theta = 0°$, 90°, 180°, etc., is not significant. The alignment of the rotation axis at right angles to the magnetic field was achieved by adjusting the crystal holder until the two peaks of the $\nu' - \nu''$ curve of Fig. 7 separated by 180° became of the same height. A very slight tilt of the rotation axis with respect to the magnetic field produced a difference of as much as 15 kc/sec. in the height of the two peaks.

A Fourier analysis of the curve of Fig. 7 was made up to the sixth harmonic. The amplitudes of the terms

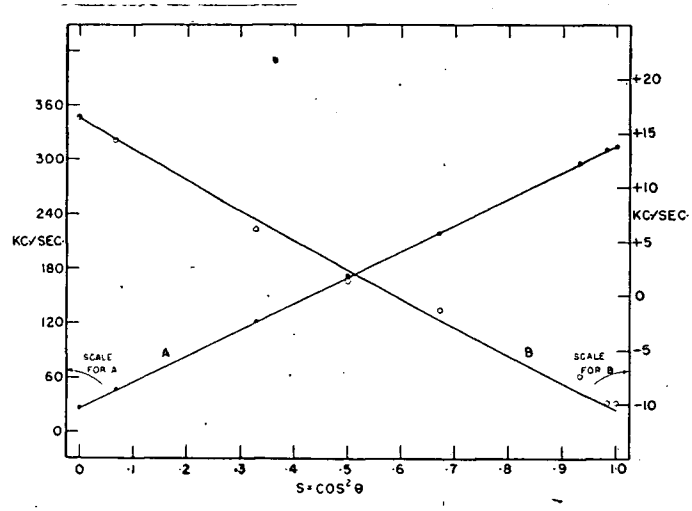

Fig. 9. The points of Figs. 7, 8 replotted as a function of $s_Y \equiv \cos^2 \theta_Y$. Each point of Fig. 9 is the average of four symmetrically situated points of Figs. 7,8. The solid straight line A is $(\nu' - \nu'')_Y = 25.7 + 290.2 s_Y$ which represents an empirical fit to the points of Fig. 9 resulting from a Fourier analysis of the curve of Fig. 7. The solid curve B is the theoretical curve $(\bar{\nu} - \nu_o)_Y = 16.2 - 28.7 s_Y + 1.9 s_Y^2$ calculated from the data obtained from curve A, from the central Al^{27} line X rotation in Ref. (23), and from spodumene sample 3X. The experimental points lying on curve B are uncertain by $\pm$ 2 kc./sec.

to face page 36

of periods predicted by the first of equations (13) for the Y rotations were: $c_Y = 0$ by the choice of the origin, and $a_Y = 170.8 \pm 0.5$ kc./sec., $b_Y = R_Y = 145.1 \pm 0.5$ kc./sec. The r.m.s. value of the amplitudes of all the other harmonics was found to be 0.43 kc./sec., which differs from zero by less than the experimental error. Expressing this in the linear form of the last of equations (13) we obtain $L_o = 25.7 \pm 1$ kc./sec., and $L_1 = 290.2 \pm 1$ kc./sec. The solid line A of Fig. 9 shows this straight line which has been empirically fitted to the experimental points of Fig. 7 replotted against $s = \cos^2\theta_Y$. Each point of Fig. 9 is the average of the four points at $\pm\theta$, $\pm(\pi + \theta)$ of Fig. 7. The points of Fig. 8 are similarly replotted in Fig. 9. The experimental accuracy in this case does not justify an attempt to obtain an independent empirical set of constants in equation (16) to fit these points. Instead of this, the theoretically expected values of these constants were calculated from the data obtained from the preceding curves, as described below. The solid curve B of Fig. 9 is this calculated curve which shows that the observed points are consistent with it.

Some information on the "inner" (m = 3/2) satellites was also obtained from the X rotation of sample No. 3X in a field of $H_o = 6129$ gauss corresponding to $\nu_o = 6.804$ Mc./sec. Zero splitting was observed at $\theta_X = 100^\circ \pm 1^\circ$ and

$\theta_X = 192^\circ \pm 1^\circ$. The expected positions for maximum splitting are then midway at $\theta_X = 146^\circ$, and 90° from the latter position at $\theta_X = 236^\circ$. The observed splittings in these two positions were $\nu' - \nu'' = \pm (885 \pm 2)$ and $\mp (856 \pm 3)$ kc./sec. respectively. Neglecting at this stage any third order effects, whose possible influence will be discussed at the conclusion of this section, substitution of these data in equation (13) gives: $\delta = 56^\circ \pm 1^\circ$, $a_X = -14.5 \pm 4$ kc./sec., $R_X = 870 \pm 4$ kc./sec., $b_X = R_X \cos 2\delta = -326 \pm 30$ kc./sec.

Table II lists the values of a, b, R obtained directly from the Y and X rotations of crystals 2Y and 3X respectively, and also computed from the above observations with the aid of identities (20). It is seen that the a and b values obtained from the two rotations agree within experimental error. Sample 3X provides a value of R_X, while sample 2Y provides better values of R_Y and R_Z than sample 3X.

TABLE II

VALUES OF a, b, R (IN KC./SEC.) IN EQUATION [13] REQUIRED TO FIT THE OBSERVATIONS ON SAMPLES 2Y, 3X. FOR SAMPLE 2Y, a_Y, b_Y WERE OBTAINED FROM A FOURIER ANALYSIS OF $(\nu' - \nu'')_Y$ GIVEN BY THE POINTS OF FIG. 7 FOR THE "INNER" SATELLITES. THE REMAINING COEFFICIENTS WERE CALCULATED FROM THE IDENTITIES [20]. FOR SAMPLE 3X, a_X, R_X, AND $\delta = 56^\circ \pm 1^\circ$ WERE OBTAINED BY OBSERVING THE POSITIONS AND AMOUNTS OF MAXIMUM POSITIVE AND NEGATIVE SPLITTINGS $(\nu' - \nu'')_X$. b_X WAS COMPUTED FROM $b_X = R_X \cos 2\delta$, AND THE OTHER QUANTITIES FROM THE IDENTITIES [20]

Axis	Sample 2Y			Sample 3X		
	X Calc.	Y Obs.	Z Calc.	X Obs.	Y Calc.	Z Calc.
a	-13 ± 1.0	171 ± 0.5	-158 ± 1.0	-14.5 ± 4	170 ± 15	-156 ± 15
b	-329 ± 1.0	145 ± 0.5	184 ± 1.0	-326 ± 30	142 ± 15	184 ± 15
R	—	145 ± 0.5	184 ± 1.0	870 ± 4	142 ± 15	184 ± 15

We now apply the theory of Chapter 2 to determine the absolute value of the quadrupole coupling constant $|C_z|$, the asymmetry parameter η, and the principal axes orientation of the ϕ_{ij} tensor at the Al^{27} sites in spodumene.

TABLE III

SUMMARY OF a_X, R_X, δ, $|C_z|$, η FROM OBSERVATIONS ON TWO SPODUMENE SAMPLES

Sample	Line component	a_X, kc./sec.	R_X, kc./sec.	δ, degrees	$\lvert C_z \rvert$, kc./sec.	η
3X	"Inner" sat.	-14.5 ± 4	870 ± 4	56 ± 1	2947 ± 20	$0.93 \pm .02$
2Y	"Inner" sat.	-13 ± 1.0	(870 ± 4)	$56.1 \pm .2$	2943 ± 15	$0.941 \pm .005$

The results are collected in Table III. In the first case values of δ, a_X and R_X are already given in Table II and $|C_z|$ and η are calculated using equations (19). In the second case the results from Table II combined with R_X from the first case give better values of a_X, and of $\delta_X = 1/2 \cos^{-1}(b_X / R_X) = 56.1^\circ \pm 0.2^\circ$. Again $|C_z|$ and η are calculated using equations (19). The best values are seen to be those from the last row. These values were substituted into the coefficients of equation (16) given in equations (22) to give curve B of Figure 9. The following expression was obtained in which the frequency is in kc./sec.

$$(\bar{\nu} - \nu_0)_\gamma = (16.3 \pm 2) - (28.7 \pm 4)s + (1.9 \pm .1)s^2 \qquad (30)$$

As mentioned above, the observed points are

consistent with this curve B but recalculation of similar coefficients for the central line Y and Z rotations indicated the possibility of a systematic error in the form of a misalignment of the rotation axes in the crystal samples. In the analysis it is assumed that the three rotation axes are mutually orthogonal, whereas actually they could be slightly tilted with respect to their intended positions. In view of this, the estimated limits of error are increased and the values finally adopted from Table III are:

$$|C_z| = 2950 \pm 20 \text{ kc./sec.}, \quad \eta = 0.94 \pm 0.01, \quad \delta = 56° \pm \tfrac{1}{2}°. \tag{31}$$

We conclude this section with some remarks on the size of the third order effects relative to the first order effects in the X rotation of crystal 3X. Substituting into equations (13), (21), (23), (24) the constants of equation (31), and $\nu_0 = 6.804$ Mc./sec., corresponding to $H_0 = 6129$ gauss used to obtain the data of Table I at zero splitting of both pairs of satellites, and the data leading to part of Table II at maximum splitting of the "inner" satellites, we obtain the following expressions for $\nu' - \nu''$ (in kc./sec.) in which the first and third order contributions are bracketed separately. For the

inner satellites we have:

$$(\nu' - \nu'')_x = (885 - 1753s_x) + (-1.53 + 79.1s_x - 236s_x^2 + 155s_x^3) \qquad (32)$$

and for the outer satellites:

$$(\nu' - \nu'')_x = 2(885 - 1753s_x) + (-0.3 - 146s_x + 440s_x^2 - 293s_x^3). \qquad (33)$$

The third order contributions in equations (32) and (33) have greatest deviations from zero near $s_x \approx 0.2$ and $s_x \approx 0.8$ amounting respectively to about +6 kc./sec. and -10 kc./sec. in the former case, and -14 kc./sec. and + 14 kc./sec. in the latter case. However, at the position of zero splitting from the first order term ($s_x \approx 0.5$), the third order contributions are only -1.5 and +0.1 kc./sec. respectively, and thus within experimental error do not influence the data of Table I. At the positions of maximum splitting of the satellites the third order contribution to the "inner" satellites is -1.5 kc./sec. at $s_x = 0$, and -3.4 kc./sec. at $s_x = 1$. These values were used to arrive at the quoted estimated errors of the measured maximum splittings.

B. Experimental check on new method of spin determination.

The spin of the Al^{27} nucleus is known from Ref. (32) to be I = 5/2. The five components of the resonance line visible in Fig. 6a would confirm this if we were sure that no weaker satellites had been missed. To convince ourselves that no weak outer components of the line have been missed, and to illustrate the new method of spin determination proposed in Chapter 2, we apply equation (18) to the values of U from Petch's work on the central line, and the values of R from Table II. The values of U were as follows: $U_X = 25.6 \pm 0.1$, $U_Y = 0.86 \pm 0.1$, $U_Z = 1.05 \pm 0.1$. We set $\nu_0 = 7.453$ Mc./sec. in equation (18) and compare the possible values of $(I + 3/2)(I - 1/2) = 3, 8, 15$ corresponding to $I = 3/2, 5/2, 7/2$ respectively, with the experimental values of $32\,\nu_0 U/R^2$, which for the X, Y, Z rotations are respectively $8.05 \pm .10$, 9.7 ± 1, 7.4 ± 1. Thus the values of spin higher than 5/2 can be definitely excluded, and the visible five components confirm I = 5/2 for Al^{27}. The large uncertainties in the experimental values of $32\,\nu_0 U/R^2$ for the Y and Z rotations are caused by the large uncertainties in U_Y, U_Z. These are poorly known because in this particular crystal the tensor ϕ_{ij} is such as to give only a very small $\cos 4\theta$ contribution to the frequency shift for the Y and Z rotations.

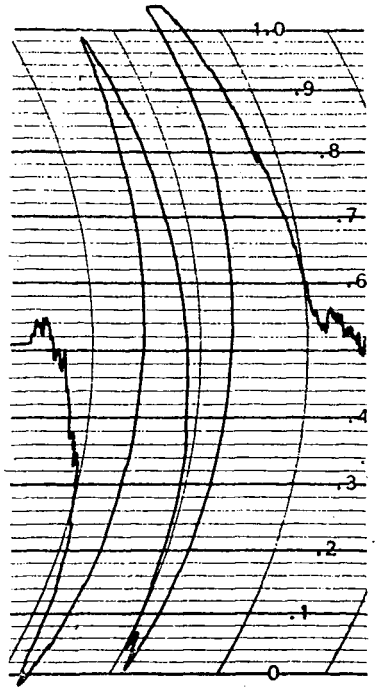

FIG. 10. Li^6 absorption derivative curve in a single crystal of $LiAl(SiO_3)_2$ showing the maximum quadrupole splitting obtainable with the crystal *b* axis perpendicular to the external magnetic field.

Frequency scale approximately 1 div. = 2.6 kc./sec.

to face page 42

C. Ratio of the Quadrupole Moments of Li^6 and Li^7.

Schuster and Pake (22) reported a value for the ratio of the magnitudes of the quadrupole moments of Li^6 and Li^7 calculated from the quadrupole splitting of the Li^6 and Li^7 magnetic resonances obtained from a single crystal of spodumene. Their crystal was mounted so as to rotate about its c axis.

The Li^7 quadrupole interaction in spodumene has been examined in detail in this laboratory by Volkoff, Petch, and Smellie and has been reported elsewhere (18). This investigation yielded complete information on the orientation of the principal axes and the degree of axial asymmetry of the field gradient tensor at the sites of the Li nuclei. The results show that maximum splitting of the Li lines is obtained when the crystal is mounted to rotate about its b axis. This exceeds by 11.5% the largest splitting obtained by a rotation about the c axis.

With a crystal so mounted, and oriented to give the maximum splitting of the Li^7 lines, the splitting of the Li^6 lines was observed. The measurements were made at room temperature in a field of about 8900 gauss. The resolution obtained is shown in Fig. 10, and represents an improvement over that reported by Schuster and Pake. It is felt that the improvement is sufficient to warrant a

recalculation of the quadrupole moment ratio. The improvement is due partly to the increase in the $\Delta\nu$ being measured and partly to a better signal-to-noise ratio which allowed the use of a smaller modulation amplitude. The measured traces were recorded with a modulation amplitude equal to approximately one-sixth of the line width at half maximum. A reduction of this modulation amplitude by a factor of 10 produced no appreciable further improvement in resolution.

From equation (10) since only first order effects are present here

$$\Delta\nu_6/\Delta\nu_7 = \tfrac{1}{2}\lambda_6/\lambda_7 = \tfrac{3}{2}Q_6/Q_7 \qquad (34)$$

or

$$|Q_6/Q_7| = \tfrac{2}{3}\Delta\nu_6/\Delta\nu_7 \qquad (35)$$

Using $\Delta\nu_{max}$ in each case, $\Delta\nu_7$ was measured to be 75.7 $\pm$ 0.5 kc./sec. in agreement with the quadrupole coupling constant $eQ\phi_{zz}/h$ for Li^7 reported in Ref. (18). $\Delta\nu_6$ was then obtained without moving the crystal by measuring the frequency difference between the positions of zero derivative of the two Li^6 lines. The lines in Fig. 10 and other similar tracings seem to be well enough

resolved so that the tail of one does not contribute to the peak of the other. The value of $\Delta \nu_6$ obtained from 30 such measurements is 2.18 ± .05 kc./sec. The quoted error is the statistical probable error.

This gives $|Q_6/Q_7| = (1.9 \pm 0.1) \times 10^{-2}$ (36)

which is significantly lower than the value $(2.3 \pm 0.2) \times 10^{-2}$ reported by Schuster and Pake. The quoted uncertainty is slightly greater than twice the statistical error. The values of neither Q_6 nor Q_7 separately appear to be known at present (33).

D. Observations on the Si^{29} Resonance.

Since the resonance spectra of Al^{27} and Li^7 and Li^6 in spodumene had been examined in this laboratory, it was decided to look for the Si^{29} resonance just for the sake of completeness.

Si^{29} is believed to have a spin of 1/2 (34) and hence a zero quadrupole moment but Sands and Pake (35) cast some doubt on this when they reported a spin determination for Si^{29}. Comparing the intensity of its magnetic resonance absorption with that of I^{127} seemed to indicate 3/2 as the correct value. They also referred to anomalous results obtained by the Stanford group. Watkins & Pound (36) however, suggest that the I^{127}

intensity observed by Sands & Pake in the KI crystals might have been reduced to a fraction of the expected value due to internal strains in the crystals. They have observed such effects. Hatton, Rollin and Seymour (37) observed a single weak resonance line in beryl ($Be_3Al_2Si_6O_{18}$) which they concluded was due to Si^{29} and reported that there was no detectable shift of the resonance on rotation of the crystal with respect to the magnetic field.

The Si^{29} resonance consisting of a single line was observed in a field of about 8930 gauss at approximately 7.575 Mc./sec. The signal-to-noise ratio of the line was about 30:1 and there was no evidence of further lines. A rotation was carried out and no shift or splitting was detected. This would seem to add to the existing evidence to confirm the spin of Si^{29} as 1/2.

Chapter 7 - Discussion.

As outlined in the Introduction, the objectives in undertaking the work described in Chapter 6 were: to check the second order and third order perturbation theory results for the dependence of the resonance frequencies on crystal orientation, to obtain higher accuracy in the values of the field gradient constants of spodumene, to check a proposed new method of spin determination, and finally to attempt to improve the accuracy of the Q_{Li^6}/Q_{Li^7} ratio.

The check on perturbation theory was obtained for a complete rotation of the crystal in the case of the "inner" satellites of the Al^{27} line in spodumene, and for a few selected positions of the "outer" satellites. It indicated that second order terms were adequate to describe the shift of the centre of gravity of the inner and outer satellites and that third order effects in the splitting of the inner satellites were of the order of 1% of the first order effects at fields of the order of 6000 gauss. In the case of the Y rotation on the inner satellites, the maximum first order splitting amounted to 316 kc./sec. and the third order effects were ignored since they were of the same order of magnitude as the experimental uncertainty. A complete rotation for the outer satellites

was not attempted. For some crystal positions these were weak, necessitating long time constants, with correspondingly long observation times and it was felt that the agreement with theory was good enough at the several selected crystal positions that no further useful information would be obtained from extending the measurements.

The values obtained for the field gradient constants in spodumene quoted in equation (31) above are slightly more accurate than those obtained previously by Dr. Petch from the central component analysis alone, but the limits of error are still greater than are inherent in the method. However, the considerable effort involved in determining the crystal axes more accurately and in orienting them more accurately with respect to the axes of rotation doesn't seem justified at present in view of the lack of any theoretical estimates of the same quantities to which they could be compared.

From the quadrupole coupling constant, when Q is known from other sources, an empirical value can be obtained for $|\phi_{zz}|$. Such empirical information on $|\phi_{zz}|$, on the asymmetry parameter η, and on the orientation of the field gradient tensor principal axes, would be useful for comparison with theoretical predictions, calculated on the basis of specific models assumed for

the crystal, if such calculations were available. Such comparisons would enable one to decide whether the bonding in a particular crystal were largely of the ionic, or the covalent type, or intermediate between the two. No theoretical calculations of the crystalline fields in spodumene have been attempted here but, in a private communication, Prof. Bersohn of Cornell University has reported that some preliminary work for the spodumene and Al_2O_3 cases was done at Cornell by one of his students. This indicated that the calculations would be of prohibitive length unless an electronic calculator were available, and they are trying to arrange for the use of one.

The experimental check on the new method of measuring nuclear spin indicates that this method will give an unambiguous spin determination. The method depends on the quadrupole coupling constant for the nucleus in question being large enough to make the second order effect in the angular dependence of the resonance frequency measurable with fair precision. In particular, one must be able to compare the amplitude of the fourth harmonic term in the second order effect with that of the second harmonic term in the first order effect. Thus, that axis of rotation of the crystal should be chosen which emphasizes

the fourth harmonic in the second order effect, and then the first order effect should be observed for a rotation about the same axis.

When referring, in Chapter 2, to spin determinations by counting line components, the statement was made that satellites might be broadened and weakened by crystal imperfections and impurities. This effect was observed by Petch et al. (23); in the first crystal samples used only the central Al^{27} line was observable. This is most likely caused by a spread in the local values of $\nabla\vec{E}$ at the various Al sites throughout the crystal due to such imperfections and impurities. In accordance with equations (13) and (15) the central component ($m = 1/2$) of the line has no first order dependence of the resonance frequency on $\nabla\vec{E}$, while the satellites ($m = 3/2$ and $5/2$) do show first order effects. Therefore local variations in $\nabla\vec{E}$ from one nuclear site to another will produce a much greater broadening of the satellites as compared with the central component, and may smear them out so as to make them unobservable. A similar explanation has been offered recently by Watkins and Pound (36) to account for the anomalously weak intensity of resonance lines of some nuclei in cubic crystals.

The ratio of the quadrupole moments of the lithium isotopes is calculated from the quadrupole coupling constants

by cancelling the ϕ_{zz} term in each. In cancelling out the ϕ_{zz} term we have assumed that the field gradient tensor at the Li^6 and Li^7 sites is the same. The two types of nuclei will be in equivalent crystallographic positions, of course. But the field experienced by the nucleus is a combined one due to the neighboring ions plus that due to the atomic electron shells and bonding electrons surrounding the nucleus itself. This latter contribution may perhaps be slightly different in the case of the Li^6 and Li^7 nuclei. In the first approximation if the two nuclei are considered as point charges there should be no difference at all. However, considering the finite size of the two nuclei, and the different charge distributions on each (as evidenced by the large differences in the experimentally observed quadrupole coupling constants), it is possible that the wave functions are distorted to some extent by the finite nucleus by amounts which differ in Li^6 and Li^7. This may, in principle, give rise to a small difference in ϕ_{zz} at the two sites.

If the bonding of Li in spodumene is assumed to be of purely ionic type, then the only effect of the local spherically symmetric electron distribution of a Li^+ ion on ϕ_{zz} will be to screen out partially the electric field due to neighboring ions. Prof. Bersohn, in the private communication referred to above, estimates this shielding

effect in the Li^{+} case to be of the order of 10%. It seems reasonable to assume that the difference in this shielding between the two isotopes will be an order of magnitude smaller. In view of this, the limits of error placed on the quadrupole moment ratio, amounting to about ± 5% , seem adequate.

PART III - EXPERIMENTAL

Pure Quadrupole Spectra

Chapter 8 - Apparatus and Experimental Procedure.

A. Super-Regenerative Oscillators - General.

It was decided to attempt to observe the pure quadrupole spectrum of Al^{27} in spodumene. Calculations of Lamarche and Volkoff (21) showed that the spectrum should consist of two lines of medium strength at 0.789 and 0.758 Mc/sec. plus a much weaker line at the sum of these frequencies. From their calculations on transition probabilities, and other calculations (25) on theoretically available signal-to-noise an approximate calculation of the signal amplitudes to be expected was made. In the work at high magnetic fields reported in Part II, which was carried out with the spectrometer previously constructed by Collins and improved by Petch, the size of the magnet gap had restricted the size of the crystal samples to about 2 c.c. For such a sample, the calculation indicated that the signals would be only of the order of the noise. Since there would be no such restriction on sample size in the pure quadrupole case, it was hoped that the gain in signals by increasing the samples

to 50 - 100 c.c. or more would be sufficient to bring them above noise level.

Larger samples would require a higher r.f. power level to give the same energy density in the sample volume. Also it was felt that the r.f. power levels being used in the Collins spectrometer were many times below what the crystal samples would stand without onset of saturation. Since, in the absence of saturation, the absorbed power is proportional to the r.f. power incident on the sample, a gain in signal-to-noise should be obtained by increasing the power level, providing that there was not a proportionate increase in the noise generated by the oscillator.

Regenerative oscillators of the Collins' type (18), or of the Watkins and Pound type (38), operate best at low power levels and the noise figure deteriorates as the level is increased, so that nothing can be gained in signal-to-noise ratio in this way. Super-regenerative oscillators have been shown (20,39) to operate well at high power levels and can be swept in frequency. They have some obvious disadvantages, including a complicated frequency spectrum which produces extra spectral lines that may be difficult or impossible to resolve in the case of wide lines at low frequencies. But in view of the fact that the quadrupole spectra of lowest frequency (as low as 1.5 Mc./sec),

which have been reported in the literature (8), have been recorded using a super-regenerative oscillator, the decision was made to build a spectrometer of this type in the hope that it could be made to operate at frequencies even below 1 Mc./sec.

A super-regenerative oscillator is a pulsed radio-frequency oscillator. It consists of a resonant circuit and a regenerator tube, plus a means of turning the oscillation on and off.

This is commonly accomplished by applying a periodic voltage wave from an external oscillator or pulse generator directly to the grid of the oscillator tube. The quenching wave, as it is called, may be a sine wave, square wave, sawtooth, or of more complicated form. The effective conductance seen by the resonant circuit will be a function of time, $g(t)$, alternately positive and negative, and equal to the sum of the positive conductance representing the inherent and coupled losses of the tuned circuit and the negative conductance supplied by the regenerator tube. Some control of the relative durations of the positive and negative periods is desirable and this may be accomplished by biasing the oscillator tube and varying the quenching wave shape.

The quenching action, when $g(t)$ is positive,

erases the effect of the previous cycle, reducing the voltage across the tank circuit to the order of thermal noise voltages. The off-time is usually made long enough compared to the decay time constant of the tank circuit (of the order of 10 to 15 times it) to allow the amplitude of the oscillations to fall to this level. As the quenching is withdrawn and g(t) goes through zero, oscillations will be initiated by the voltages remaining in the tuned circuit and the envelope of these oscillations will rise exponentially as g(t) becomes negative. The tube is left on long enough to include many r.f. cycles and for the purpose of this description we will assume that it is left on long enough for the oscillations to level off at the saturation amplitude U_{max}. This is called the logarithmic mode. The time taken to reach U_{max} depends sensitively on the minimum amplitude U_{min} from which the oscillations build up. When signals from an external transmitter are present, the average U_{min}, consisting of signal plus noise, is increased and the time average of the oscillation amplitude increases. Any modulation of the signal will appear as a change in this time average and may be detected, amplified, and presented using standard procedures.

Analysis (40) shows that the output is a greatly amplified reproduction of the signal-plus-noise

amplitudes. If a perfect square-wave quenching voltage is assumed, the gain is given in Ref. (40) as:

$$\text{Gain} = f_q U_{max} 2L/R_T \ln(V_n + V_s)/V_n$$

where f = the quench frequency

L = tank coil inductance

R_T = net series tank resistance = $R + R_n$

R = series loss resistance of tank circuit

R_n = negative series resistance representing the regenerator tube

V_n = noise voltage at instant that oscillations start

V_s = signal " " " " " "

This gain can be as much as 10^6. For a sine-wave quenching voltage the gain is higher. The same gain law holds but is more difficult to apply since R_T can not be assumed constant. The effective R_T is smaller but the maximum f_q is also smaller.

In Refs.(41,42) a slightly more general treatment of the super-regenerator is given. Expressions are developed for selectivity and sensitivity which can be applied to any quench wave form. In (41) Bradley concludes that the narrowest band and greatest sensitivity as well as the best signal-noise ratio appear to be obtainable with a conductance function g(t) of the following form: g(t) has a large positive value for the quenching period, which is made as short as is consistent with thorough quenching. This is

followed by a period in which $g(t) = 0$. This period is made as long as possible. In the third period $g(t)$ should become quite negative very quickly so as to give maximum amplification of the voltages existing at the end of the second period. The third period should be as short as is practical.

The spectrum of the r.f. output of a super-regenerative oscillator is very complex. If the quenching is not complete (so that there is coherence between the r.f. oscillations in successive pulses), the spectrum consists essentially of a central carrier frequency with side-band frequencies, of decreasing intensity, displaced by integral multiples of the quench frequency f_q. The intensity distribution will not, in general, be symmetrical about the carrier frequency and the rate of fall-off in intensity will depend on the Q of the circuit. In addition to this amplitude modulation there is a frequency-modulation effect, of much smaller order, since the resonant frequency depends on tube voltages, damping, etc.

If quenching is complete, so that there is no coherence between pulses, in the absence of signals the spectrum will be continuous and extend over approximately

the same band-width as in the coherent case. Now if signals are present, the phase relationship between successive pulses is determined by the signal and the spectrum is again a set of discrete frequencies but the apparent carrier frequency is now a function of the signal frequency.

The above description of a super-regenerative receiver has been given, purposely, in terms of receiving radio signals from an external transmitter.

The detection of nuclear resonance absorption by a super-regenerative spectrometer can take place by two different processes. When a sample is placed in the tank coil and the oscillator frequency is swept through the resonant frequency, assuming the magnetic field or the frequency is being modulated in the usual way, the absorptive or χ'' component of the nuclear susceptibility produces amplitude modulation of the carrier which may be detected by standard methods. This process is not related to the reception of radio signals referred to above.

Roberts (43) suggested, that in addition to this effect, there might be voltages induced in the tank coil by precessing nuclei as in the nuclear induction technique. These voltages would play the same role as signals from an external transmitter and the analysis for this process would be the same as for radio reception. It now seems to be

accepted that this is the important process, for the case of incoherent operation (39) at least. Dean (20) gives convincing arguments in favor of this picture and also feels that it is the important process for coherent operation. However, Williams (44), Gutowsky et al. (45) describe their results in terms of the straight absorption process.

The voltage induced by the precessing nuclei is given by $\Delta U \simeq -4\pi\chi'' Q' \alpha U_{max}$ where Q' is the quality factor of the tank circuit and α is a factor somewhat less than unity correcting for the intermittent nature of the r.f. field H_1 and for variations in H_1 throughout the coil volume. An essential part of this picture is that the transverse relaxation time T_2^* be long enough so that a large degree of the spin coherence obtained during one on-period remains at the beginning of the succeeding on-period. The off-time for a typical case (10 to 15 times the decay time constant) is of the order of 10 μ secs. The inverse line width $2\pi/\gamma\Delta H$ gives a measure of the transverse relaxation time. For the Al lines in spodumene using the observed line width of the order of $\Delta H \simeq 10$ gauss this is of the order of 100 μ secs. or about 10 times the necessary off-period.

The spectrum in this case in the presence of signals, will consist of discrete frequencies because of

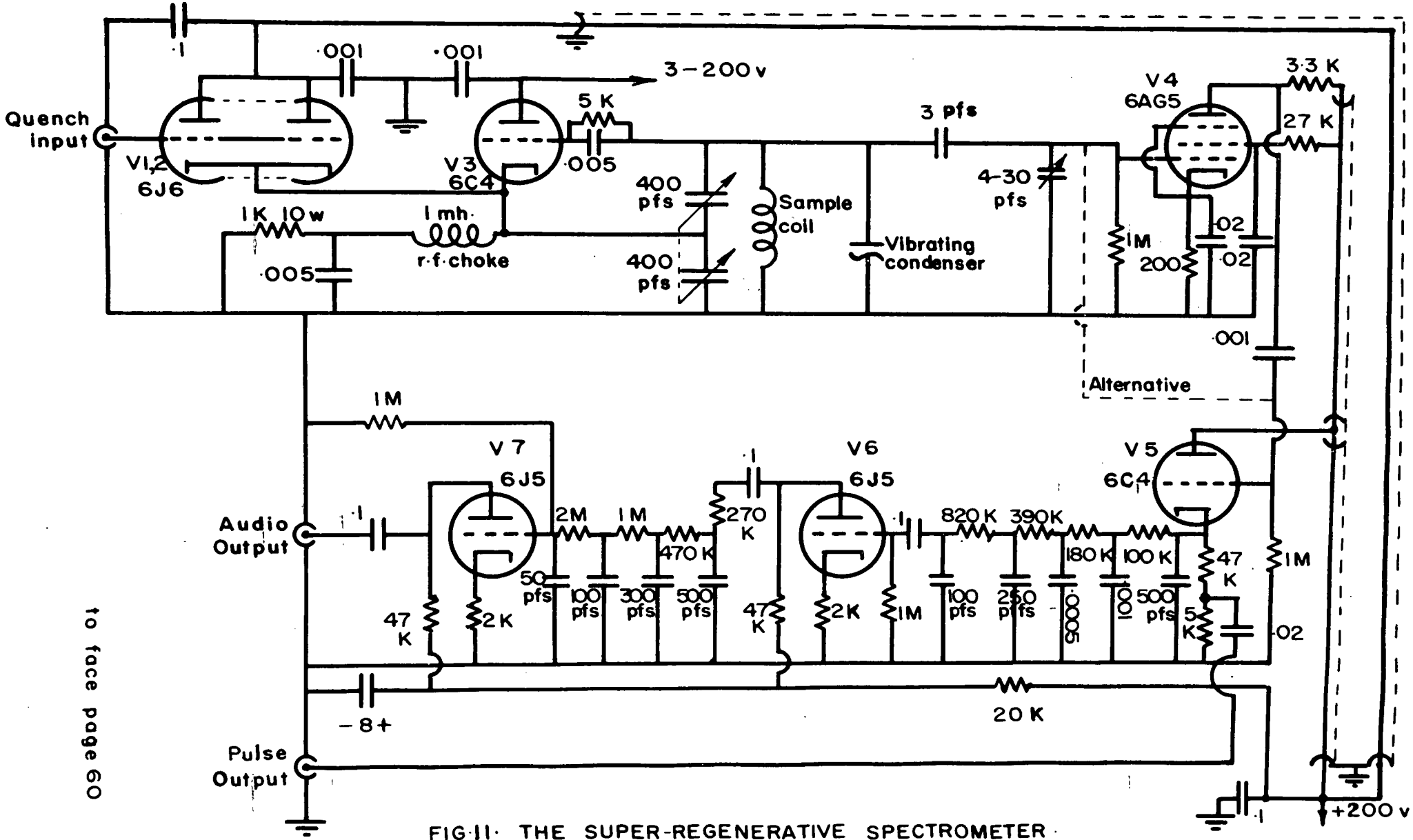

FIG·11· THE SUPER-REGENERATIVE SPECTROMETER·

to face page 60

the apparent coherence introduced by the signals. As the oscillator is swept through the region of a nuclear resonance each of these frequencies, when coincident with the transition frequency, will produce a resonance signal. A single-line nuclear resonance spectrum will then appear as a multiple-line spectrum, the number of lines depending on the band width of the tuned circuit and the quench frequency f_q. The line shapes depend on the phase relation between ΔU and U_{min} and in general will be mixtures between absorption and dispersion curves.

B. The Super-Regenerative Oscillator Used.

The circuit of the super-regenerative oscillator, which was constructed, is shown in Figure 11. The basic circuit was designed by Dean (20) for use in the region of 30 Mc./sec. Suitable modifications were made to allow its use in the region of .75 Mc./sec. to 3 Mc./sec. In addition to these modifications, provision was made for operating the oscillator at low r.f. levels and a r.f. amplifying stage was added, preceding the detector, for low level operation. This is by-passed for high level operation.

The oscillator is the grounded-plate version of the Colpitts oscillator. The quenching action is as follows: the two halves of a 6J6 (V1,2), in parallel, have their cathodes tied to the cathode of the oscillator tube, V3. The 6J6

plates are by-passed to ground for r.f. When a positive pulse from the external quenching circuit is applied to the grid of V1,2 the additional cathode bias shuts off V3, since its grid-leak condenser does not discharge immediately. The time constant of the grid leak must be short enough for the bias to recover before the quench is removed but, of course, long enough so as not to be able to follow the r.f. oscillations.

At the same time as V3 is cut off, the cathode input impedance of V1,2 is shunted across part of the tuned circuit. This large positive conductance shortens the decay time constant of the tank circuit and aids in quickly damping out the free oscillations.

It is important that this impedance should not have any damping effect during the oscillation portion of the cycle and to insure this, the grid of V1,2 must be made very negative - of the order of - 150 volts. A fixed bias that may be set from 0 to -90^{V} is provided by a battery and potentiometer. The overall positive to negative swing of the quench voltage wave should be about 150 volts.

The vibrating condenser in parallel with the tank circuit provides a means of frequency - modulating the oscillator. This is an alternative to field modulation

that is convenient for oscilloscope presentation of strong resonances. Dehmelt (39) has also used this type of modulation for chart recording of resonances but it is not as satisfactory for this as is the field modulation.

A variable capacity-divider, following the tank circuit, allows some control of the fraction of the tank voltage applied to the grid of the r.f. amplifier V4, or to the grid of the infinite impedance detector V5. The time constant of the R and C combination, in the cathode ov V5, is selected to allow the cathode to follow the pulse envelope. Biasing considerations will be the main factor in determining R, but its value should be chosen so that the C giving the desired time constant is not too small. There is a greater tendency for V5 to act as an oscillator if this C is small. The capacity-divider referred to above decouples V5 from the tuned circuit to a certain extent and also helps to prevent such oscillations.

The output from the cathode of V5 is fed into a 4-section, RC filter network which integrates the pulse areas. The time constant of these is chosen to suppress the quench frequency. Part of the output from the cathode of V5 is taken to a pulse-output terminal. This is displayed on an oscilloscope and is an essential aid in

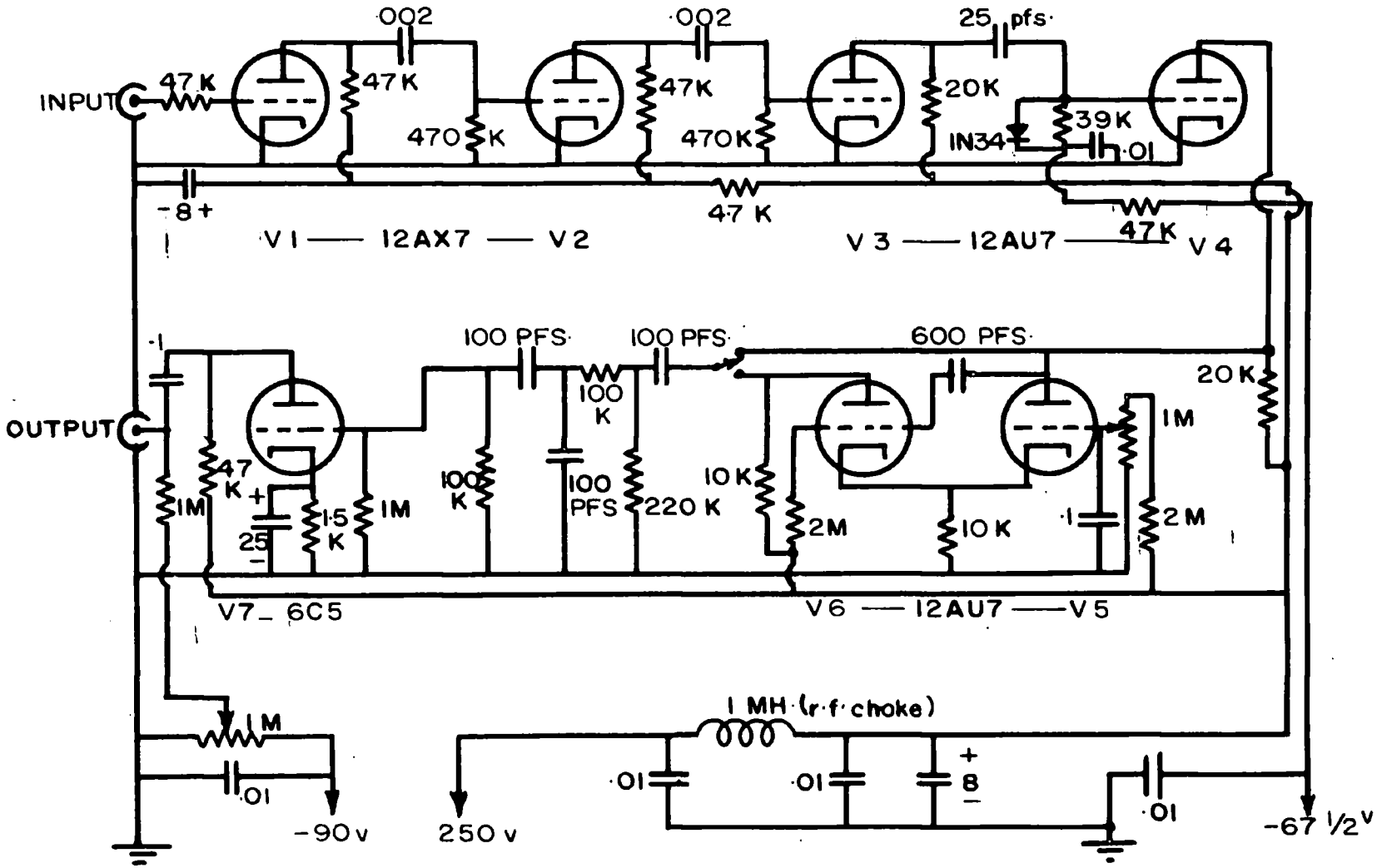

FIG. 12. THE QUENCHING CIRCUIT.

to face page 63

adjusting the oscillator. The output from the network will contain, chiefly, frequency components centred about the modulation frequency, f_m. This is amplified in a low gain audio stage, V6. Following V6 is a second filtering network similar to the first and another low gain audio stage, V7.

C. The Quenching Circuit.

The quenching circuit shown in Figure 12 is also a modification of one used by Dean (20). The input to the circuit is provided by a Hewlett-Packard audio oscillator. For the work described here, the frequency of this input, f_q, varied from 2 kc./sec. to 20 kc./sec. but with minor modifications the circuit was used for quench frequencies up to 100 kc./sec.

The first three triode sections (V1, V2, V3) square the sine-wave input. They are followed by a differentiating network. The resulting positive and negative pips appear at the grid of V4 which has a fixed negative bias, well below cut-off. Therefore only the positive pip affects the tube current. The 1N34 diode was added across the 39K resistor to suppress the effect of the negative pip further.

The output pip from V4 triggers the "one-shot" multivibrator formed by V5 and V6. With no input, V5 is

cut off and V6 is conducting. V5 and V4 have a common plate load. Thus the positive pip at the grid of V4 appears as a negative pip at the plate of V5 and the grid of V6, initiating the change to the metastable state. The duration of this state is determined by the R and C values in the grid of V6 and the setting of the potentiometer in the grid of V5. The output, taken from either plate, is then essentially a square wave in which the relative duration of the positive and negative portions may be varied.

In Dean's original circuit this square wave formed the quenching voltage. After some amplification and smoothing in V7, it was rounded somewhat by a 10K resistor and the capacitance of a short length of cable, before being applied to the grids of the 6J6. This arrangement was also tried here, before the modifications shown in Figure 12 were made. The combination of differentiating and integrating networks, shown following the multivibrator, was inserted in an attempt to reproduce an approximation to the optimum conductance wave form described by Bradley (41). The values of R and C were chosen so that the "differentiation" and "integration" would be very poorly done. The resulting wave shape was then amplified in V7 and applied to the 6J6 grids.

A comparison of the signals obtained with this quenching wave shape and with the "rounded square-wave"

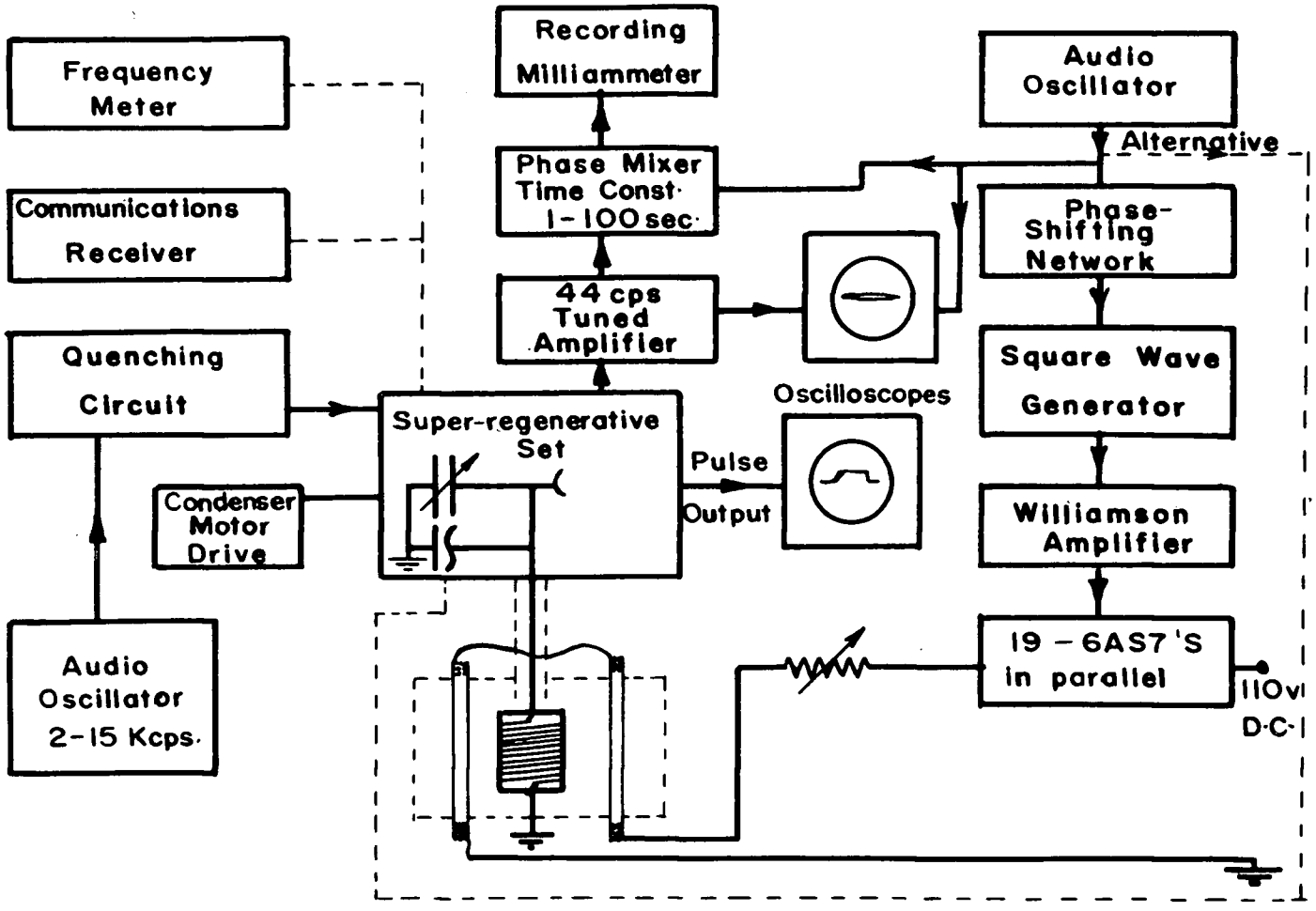

FIG. 13. BLOCK DIAGRAM OF THE SUPER-REGENERATIVE SPECTROMETER.

to face page 65

was made in the case of D signals from D_2O displayed on the oscilloscope. No marked difference was noted. However, the author feels that no fair comparison can be made on the basis of this brief check.

The circuit as shown was used for the work described in Chapter 9.

D. Modulation Methods.

Figure 13 shows a block diagram of the spectrometer. With the exception of the method of modulating the signals, the recording systems used for the pure quadrupole work were similar to the one used in the magnetic resonance work and described in Ref. (18). No further description of them is needed here. The method of field modulation used for the magnetic resonance work is also described in Ref. (18).

To record the pure quadrupole resonances, an on-off square-wave magnetic field at 44 c.p.s. was applied to the sample. During the on-period, the resonance is smeared out by the Zeeman splitting of the levels and 44 c.p.s modulation of the signal results. There is no particular significance in the choise of 44 c.p.s. as the modulation frequency. Because of the time constant of the modulation coils, a square-wave field is more easily

produced at low frequencies. An available audio amplifier, originally tuned at a higher frequency, tuned at 44 c.p.s. after minor modifications, so this frequency was used.

In some cases the field was applied by means of a solenoid; in other cases Helmholtz coils were used. The intensity of the smearing fields was about 25 gauss as this was the maximum obtainable with the equipment as it was first set up. This field seemed adequate for smearing the Cl^{35} resonances, as observed on the oscilloscope, but it is not so certain that it is adequate in the case of wide lines. Dehmelt (39) uses smearing fields of about 100 gauss. Watkins (38) reported using field intensities of about 25 gauss on N^{14} resonances but these were very narrow lines and the "negative wings" were quite pronounced indicating incomplete smearing.

The current for the modulation field was supplied by a 110 volt battery or d.c. generator. The d.c. voltage was applied to the plates of a bank of 19 - 6AS7's in parallel. The modulating coils plus a variable resistance formed the cathode load of the 6AS7's. A square-wave voltage with a peak-to-peak amplitude of about 200 volts was then applied to the grids, cutting the tubes off for half of each period. To supply the square-wave, a Hewlett-Packard audio oscillator was used to supply the input to a simple square-wave generator circuit (46). The output

of this was fed into a Williamson amplifier (47), which was provided with a dummy load matched to the output impedance of its step-down output transformer. This assured best reproduction of the square wave input. The square-wave to drive the 6AS7 grids was then taken, via a coupling capacitor, from one side of the output transformer primary, where the voltage amplitude is about 25 times the secondary output voltage.

E. Frequency Measurement.

Accurate measurement of nuclear resonance frequencies in the case of chart-recorded signals is difficult to attain. The method, described in Chapter 5 for the c.w. oscillator, is not suitable because of the possibility of confusing the various harmonics with the central frequency and because the frequency in each case is not sharply defined, but "fuzzy", due presumably to frequency-modulation effects. This makes it impossible to get a sharply defined zero-beat with a frequency meter. If the quench is turned off, the c.w. oscillation frequency can be measured, but this again does not coincide exactly with the central frequency when the quench is on.

The method used was as follows: The oscillator drive and chart drive were stopped simultaneously. The quench was then turned off and the c.w. frequency located.

Then the quench was turned on again and the central frequency was measured as accurately as possible and a marker was made. This process was repeated in the neighborhood of the strongest resonance and linear interpolation used as before.

Chapter 9 - Experimental Results.

A. Preliminary testing of the spectrometer.

The super-regenerative spectrometer described in the previous chapter was first tested for low-frequency operation as a magnetic resonance spectrometer using the magnet and modulation equipment described in Ref. (18). The crystal used, in most cases, was the milky spodumene crystal referred to in Chapter 7, with which only the central Al^{27} line was visible. This was chosen because the multiple-line spectrum produced by the super-regenerator is easier to interpret if it is due to a single nuclear resonance, and at this time we were chiefly interested in studying the operation of the spectrometer.

As was expected, it was found that much higher values of H_1 could be used without saturating the samples. With the c.w. spectrometers (30, 38) the H_1 applied to the sample is usually a few milligauss. With the super-regenerative spectrometer r.f. field intensities of the

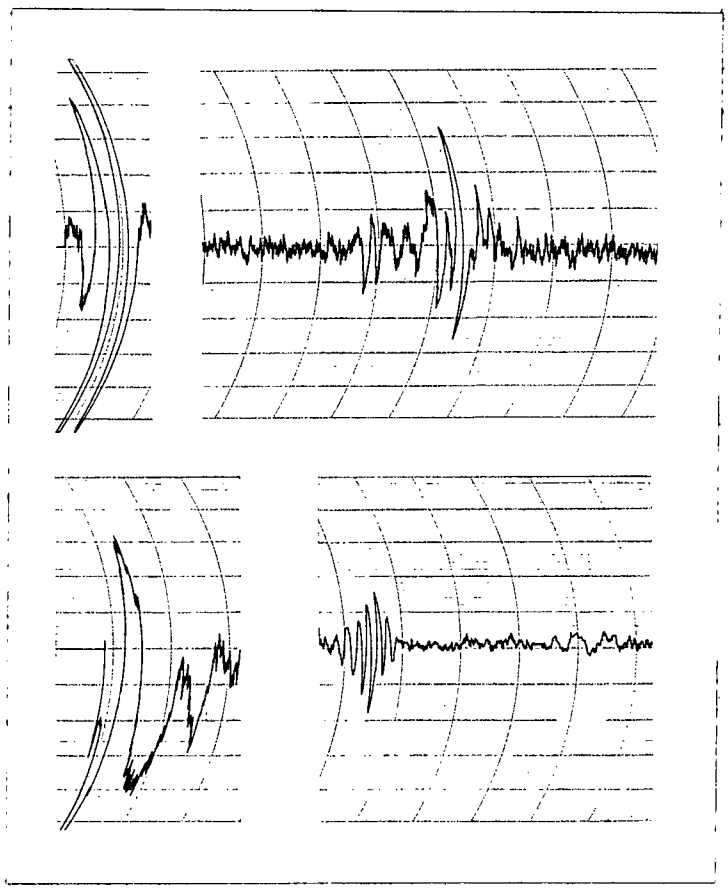

Fig. 14. Selected derivative curves for Al^{27} and Li^{7} in spodumene, recorded with the super-regenerative spectrometer. Figs.14a and 14b were recorded using a magnetic field of 1500 gauss corresponding to an unperturbed Larmor frequency for Al^{27} of $\nu_o = 1.686$ Mc./sec. In Fig. 14a the central Al^{27} line in the milky spodumene is recorded at about 1.6 Mc./sec.In Fig.14b the central and inner satellites are shown centered at about 1.6 Mc./sec.The quench frequency in each case is 10 kc./sec. The frequency scale in Fig.14a is 25 kc./sec. per division and in Fig.14b is 50 kc./sec. per division. Figs.14c and 14d were recorded using a magnetic field of 1100 gauss corresponding to an unperturbed Larmor frequency for Al^{27} of $\nu_o = 1.193$ Mc./sec. and for Li^{7} of $\nu_o = 1.780$ Mc./sec. Fig.14c shows the central Al^{27} line in the milky spodumene at about 1.2 Mc./sec. The quench frequency was 7 kc./sec. and the frequency scale is about 12.5 kc./sec. per division. Fig.14d shows the Al^{27} resonance centered at about 1.2 Mc./sec. and the Li^{7} resonance centered at about 1.78 Mc./sec. The frequency scale averages about 150 kc./sec. per division and the quench frequency is 15 kc./sec.

to face page 69

order of 0.5 gauss or more have been used without apparent saturation of the Al^{27} resonance in spodumene.

The central Al line from the milky spodumene crystal was observed at several values of the magnetic field H_o, the lowest value used being about 1100 gauss. For comparison, a few traces were recorded using a clear crystal of spodumene, in which satellites were visible. The volume of this crystal was slightly less than half that of the milky crystal. Representative traces are shown in Figure 14. The traces of Figures 14a and 14b were recorded in a field of about 1500 gauss. Figure 14a shows the central Al^{27} line obtained with the milky crystal at about 1.6 Mc./sec. In Figure 14b, obtained with the clear crystal, the central line frequency is approximately the same. The signal amplitude is down mainly because of reduction in sample volume. One "inner" satellite is visible but the other is so close to the central line that the super-regenerative satellites of each overlap. Figure 14c was recorded with the milky crystal using a field of about 1100 gauss. The approximate frequency of the Al^{27} resonance in this case was 1.2 Mc./sec. Figure 14d, also recorded at 1100 gauss but with the clear crystal, is reproduced here as an indication of the stability of the spectrometer. The frequency range covered in the trace is over 600 kc./sec. At the right are the Al^{27} resonances centered at about

1.2 Mc./sec. and at the left are the Li^7 resonances centered at about 1.78 Mc./sec. The signal amplitudes are down because of the high sweep rate.

It is of interest to compare the signal-to-noise obtained with this spectrometer, for example in Figure 14b, with that obtained with the Collins spectrometer using a sample of comparable size. At 2.3 Mc./sec., the signal-to-noise of the Al^{27} central line with the latter spectrometer was about 2:1. At 1.6 Mc./sec. the theoretically-available signal-to-noise would be a factor of 2 lower than at 2.3 Mc./sec. so the central line would be down to the order of the noise.

Having established that the super-regenerative spectrometer would detect comparatively weak nuclear resonances at frequencies as low as 1 Mc./sec., the testing was discontinued and searches for pure quadrupole resonances were begun.

B. Pure Quadrupole Spectra.

The search for the pure quadrupole Al^{27} resonances in spodumene, the calculated frequencies of which were 0.758 Mc./sec. and 0.789 Mc./sec., has so far been without success. A search for one of the pure quadrupole Al^{27} resonances in Al_2O_3, predicted to occur at 0.718 Mc./sec. and unsuccessfully

searched for by Pound (17), has also been made without success. Polycrystalline samples, with volumes ranging up to about 500 c.c., have been used. The author feels that, although these resonances are probably quite weak, they might be detectable with the super-regenerative spectrometer when more experience is gained in the operation of the spectrometer at low frequencies.

The spectrometer has detected a pure quadrupole resonance at 1.27 ± .01 Mc./sec. in $Na_2B_4O_7.4H_2O$ (kernite). Mr. H. Waterman, in this laboratory, is investigating the magnetic resonance spectrum of B^{11} in kernite, in a magnetic field of about 7000 gauss. Preliminary results indicate that there are 4 non-equivalent boron positions in a unit cell. An analysis of the dependence of the frequencies of the B^{11} lines, on crystal orientation, for one of these four positions, gave an estimate of the quadrupole coupling constant and of η . From these values, a pure quadrupole transition was predicted at a frequency of 1330 ± 80 kc./sec. A private communication, from Prof. W. Proctor of the University of Washington, states that Mr. Blood of that Department has calculated a pure quadrupole line at 1250 kc./sec. on the basis of his high field measurements. The transition observed is consistent with this predicted line but definite assignment of this observed line to B^{11} can not be made without further

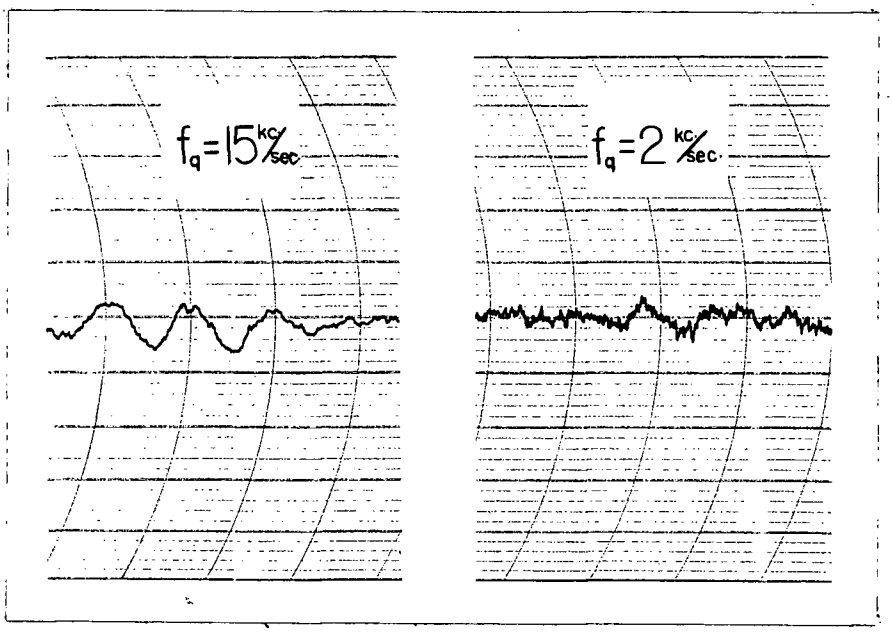

Fig. 15. A recorded pure quadrupole resonance in $Na_2B_4O_7.4H_2O$. In Fig. 15a the quench frequency is 15 kc./sec. and the frequency scale about 29 kc./sec. per division. In Fig. 15b the quench frequency is 2 kc./sec. and the frequency scale the same as in Fig. 15a. The measured frequency of the peak in Fig. 15b is 1.27 Mc./sec. and the pattern in Fig. 15a is centered at this same frequency. The pattern of the resonance in Fig. 15a is complicated due to the fact that the resonances are a mixture of absorption and dispersion curves which are not completely resolved and not completely smeared out during the "on-field" part of the modulation cycle.

to face page 72

investigation. The magnetic resonance spectrum of Na^{23} in kernite has not yet been examined. It is possible that Na^{23} might give rise to a pure quadrupole resonance in this same region. Prof. Itoh, of Osaka University, in a private communication, has predicted on the basis of high field work a Na^{23} pure quadrupole transition of 1.23 Mc./sec. in $Na_2S_2O_3.5H_2O$. Since the values of $|\phi_{33}|$ remain of the same general order of magnitude in various compounds of the same general type, the possibility that the observed transition is due to Na^{23} cannot at this stage be excluded.

Recorded traces of the observed resonance are shown in Figure 15. In Figure 15a, with a quench frequency of 15 kc./sec. the super-regenerator satellites are not resolved. In Figure 15b the quench frequency has been reduced to 2 kc./sec. This has caused the super-regenerator satellites to fall within the resonance line but has also reduced the gain by a factor of 4 or 5. The pronounced "negative wings" are believed to be due to an inadequate smearing field.

The quoted uncertainty in the frequency of this line has been made quite high because of the difficulties in frequency measurement discussed in Chapter 8.

The observation of a pure quadrupole line at 1.27 Mc./sec., which is the lowest pure quadrupole frequency

reported in the literature to date, concludes the preliminary stage of the investigation of the suitability of super-regenerative detectors for the observation of pure quadrupole spectra in this low frequency region. Further extensions and applications of this technique will be left for future investigations.

REFERENCES

(1) Bloch, F., Hansen, W.W. and Packard, M., Phys. Rev. 70, 474 (1946)

(2) Purcell, E.M., Torrey, H.C. and Pound, R.V., Phys. Rev. 69, 37 (1946)

(3) Pake, G.E., J. Chem. Phys. 16, 327 (1948)

(4) Van Vleck, J.H., Phys. Rev. 74, 1168 (1948)

(5) Kruger, H., Z. Phys. 130, 371 (1951)

(6) Bersohn, R., J. Chem. Phys. 20, 1505 (1952)

(7) Cohen, M.H., Ph. D. Thesis, University of California (1952)

(8) Dehmelt, H.G., Z. Phys. 133, 528 (1952)

(9) Dehmelt, H.G., Z. Phys. 130, 356 (1951)

(10) Dehmelt, H.G., J. Chem. Phys. 21, 380 (1953)

(11) Dehmelt, H.G., Phys. Rev. 91, 313 (1953)

(12) Watkins, G.D. and Pound, R.V., Phys. Rev. 85, 1062 (1952)

(13) Dehmelt, H.G. and Kruger, H., Z. Phys. 129, 401 (1951); 130, 385 (1951)

(14) Dean, C., Phys. Rev. 86, 607 (1952)

(15) Livingstone, R., J. Chem. Phys. 20, 1170 (1952)

(16) Carr, E.F. and Kikuchi, C., Phys. Rev. 78, 1470 (1950)

(17) Pound, R.V., Phys. Rev. 79, 685 (1950)

(18) Volkoff, G.M., Petch, H.E. and Smellie, D.W., Can. J. Phys. 30, 270 (1952)

(19) Kruger, H. and Meyer-Berkhout, U., Z. Phys. 132, 221(1952)

(20) Dean, C., Ph. D. Thesis, Harvard University (1952)

(21) Lamarche, G. and Volkoff, G.M., Can. J. Phys. 31, 1010 (1953)

(22) Schuster, N.A. and Pake, G.E. Phys. Rev. 81, 157 (1951)

(23) Petch, H.E., Cranna, N.G. and Volkoff, G.M. Can. J. Phys. 31, 837 (1953)

(24) Cranna, N.G., Can. J. Phys. 31, 1185 (1953)

(25) Bloembergen, N., Purcell, E.M. and Pound, R.V. Phys. Rev. 73, 679 (1948)

(26) Volkoff, G.M.,Can. J. Phys. 31, 820 (1953)

(27) Casimir, H.B.G. On the Interaction Between Atomic Nuclei and Electrons (De Erven F. Bohn N.V., Haarlem, 1936)

(28) Lamarche, G. M.A. Thesis, University of British Columbia(1953)

(29) Townes, C.H. and Dailey, B.P., J. Chem. Phys. 20, 35(1952)

(30) Collins, T.L., Ph. D. Thesis, University of British Columbia (1950)

(31) Petch, H.E., Ph. D. Thesis, University of British Columbia (1952)

(32) Lew, H., Phys. Rev. 76, 1086 (1949)

(33) Sternheimer, R.M. and Foley, H.M., Phys. Rev. 92, 1460 (1953)

(34) Weaver, H.E., Phys. Rev. 89, 923 (1953)

(35) Sands, R.H. and Pake, G.E., Bull. Am. Phys. Soc. 27, No. 5, D10, (1952)

(36) Watkins, G.D. and Pound, R.V., Phys. Rev. 89, 658 (1953)

(37) Hatton, J., Rollin, B.V. and Seymour, E.F.W., Phys. Rev. 83, 672 (1951)

(38) Watkins, G.D.,Ph. D. Thesis, Harvard University (1952)

(39) Dehmelt, H., Am. J. Phys. 22, 110 (1954)

(40) Van Voorhis, S.N., Microwave Receivers. Vol. 18, M.I.T. Radiation Lab. Series (McGraw-Hill,New York, 1948)

(41) Bradley, W.E., Electronics, 21, 96 (1948)

(42) Hazeltine, A., Richman, D. and Loughlin, B.D., Electronics, 21 , 99 (1948)

(43) Roberts, A., Rev. Sci. Inst. 18, 845 (1947)

(44) Williams, D., Physica, 17, 454 (1950)

(45) Gutowsky, H.S., Meyer, L.H. and McClure, R.E., Rev. Sci. Inst. 24, 644 (1953)

(46) Cruft Electronics Staff, Electronic Circuits and Tubes, p. 820 (McGraw-Hill, New York, 1947)

(47) Williamson, D.T.N., Wireless World, August (1949)